Journal of Wind Engineering & Industrial Aerodynamics 257 (2025) 105964

Contents lists available at ScienceDirect

Journal of Wind Engineering & Industrial Aerodynamics

journal homepage: www.elsevier.com/locate/jweia

Post-critical flow over arrangements of multiple rough cylinders

David Burton *, Gershom Easanesan, Anil Pasam, Christopher Brown, Daniel Tudball Smith, Mark C. Thompson

Fluids Laboratory for Aeronautical and Industrial Engineering (FLAIR), Department of Mechanical and Aerospace Engineering, Monash University, Victoria, Australia

ARTICLE INFO

Keywords:
Cylinder
Drag
Post-critical
Roughness
Reynolds number

ABSTRACT

In this study, a comprehensive set of wind-tunnel experiments was undertaken to gain insight into the variation of force coefficients (lift and drag) across different wind angles and spacings for equidistant cylinder arrangements (two, three, and four cylinders) in post-critical flows. The effect of both the cylinder spacing and wind incidence angle was examined for a roughness Reynolds number of approximately 770. The broad trends in the force coefficients previously observed for cylinders in sub-critical flow are shown to persist in post-critical flow, although the magnitudes of the coefficients are different, particularly for the maximum lift coefficient. Additionally, several methods are examined for predicting the forces experienced by multiple cylinder combinations using data obtained from the two-cylinder case. In general, these methods provide good predictions for large cylinder spacings but are inconsistent when the cylinders are spaced closer together.

1. Introduction

Circular cylinders are amongst the most commonly studied bluff bodies due to their simple geometry and many practical purposes. The aerodynamic behaviour of isolated, smooth cylinders is well-established and will not be addressed in detail here; a detailed description of smooth cylinder flow can instead be found in the work of Niemann and Hölscher (1990). Of greatest relevance here is the common classification of the flow as sub-critical, critical, supercritical or post-critical based on the Reynolds number ($Re = U_\infty d/\nu$, where U_∞ is the free-stream velocity, d is the cylinder diameter and ν is the kinematic viscosity). For smooth cylinders, in the sub-critical range ($Re \approx 10^4 - 10^5$), the drag remains relatively stable with Reynolds number, before falling rapidly as the Reynolds number increases into the critical range. Beyond a critical Reynolds number ($Re_{crit} \approx 5 \times 10^5$), where the drag reaches a minimum, the flow enters the supercritical regime, where the drag recovers but is accompanied by irregular vortex shedding. As the Reynolds number increases further into the post-critical regime, the drag coefficient becomes less sensitive to further changes to the Reynolds number and regular vortex shedding is restored. Many large-scale cylindrical structures experience sufficiently large Reynolds number flows to be well within the post-critical range. However, due to limitations of scale and wind speeds in experiments and computational costs for simulations, it is difficult to reproduce these flows in numerical and laboratory settings.

In large-scale engineering applications, the surfaces of cylindrical structures exposed to the wind are typically not smooth. Relative to a smooth cylinder, rough cylinders produce higher drag in the post-critical regime and also produce a higher minimum drag (Fage and Warsap, 1929; Achenbach, 1971). Additionally, the critical Reynolds number is lowered, resulting in post-critical flow occurring at lower Reynolds numbers. Szechenyi (2006) suggested that increased surface roughness could be used to "artificially" increase the Reynolds number and induce post-critical flow. They found that a Reynolds number based on the size of the roughness elements on the cylinder surface (instead of cylinder diameter) was a good descriptor governing the drag in the supercritical and post-critical regimes. This concept was recently revisited by Pasam et al. (2023) who conducted experiments on cylinders with different surface roughness values at Reynolds numbers up to 6.8×10^5. They found that flow quantities including the mean drag coefficient, Strouhal number and fluctuating lift coefficient were a function of the roughness Reynolds number, which aligns with the findings of Szechenyi. Building on these results, the present study uses surface roughness to produce post-critical flows at moderate Reynolds numbers to provide insight into flows relevant to large-scale structures.

Many engineering applications such as cooling and flare towers, large circular frame structures, office buildings, and chimneys can involve arrangements of multiple cylinders, where the cylinder-to-cylinder interactions affect the load on individual cylinders within the arrangement and on the structure as a whole. For this reason, the interactions of circular and non-circular cylinders remains a topic of current relevance (e.g., Wang et al. (2022), Dubois and Andrianne (2022),

* Corresponding author.
E-mail address: david.burton@monash.edu (D. Burton).

https://doi.org/10.1016/j.jweia.2024.105964
Received 6 August 2024; Received in revised form 4 November 2024; Accepted 18 November 2024
Available online 9 December 2024

and Zhou et al. (2024)). A volume of work has been undertaken on staggered two-cylinder arrangements in sub-critical flow, including reviews by Zdravkovich (1977), and more recently by Sumner (2010). Supercritical flows have also been examined to some degree (e.g. Gu, 1996). However, post-critical flows on staggered rough cylinders, which are the focus of the present study, remain largely unexplored.

Based on flow behaviour, two-cylinder sub-critical flows were described by Sumner et al. (2005) as closely spaced ($s/d < 1.5$), moderately spaced ($1.5 \geq s/d \geq 2.5$) or widely spaced ($s/d > 2.5$), where s is the centre-to-centre distance between the cylinders. The closely-spaced cylinders behaved similarly to a single bluff body, with the same Strouhal number measured for both cylinders. Large variations in the aerodynamic forces were observed as the wind direction was changed for these configurations. The moderately-spaced cylinders produced force coefficients on the upstream cylinder which were relatively insensitive to the wind direction, but more complex behaviour was observed on the downstream cylinder. Both the closely- and moderately-spaced cylinders produce a peak in the lift-force magnitude on the downstream cylinder when the cylinders were close to in-line, which coincides with a local minimum drag coefficient on the downstream cylinder and a local maximum in the drag coefficient on the upstream cylinder. These features were absent for the widely-spaced cylinders. Those cases saw forces on the upstream cylinder that were similar to those on an isolated cylinder. For these spacings, the downstream cylinder produced a minimum drag coefficient when the cylinders were in-line with each other. Additionally, a single Strouhal number was observed on both cylinders and was attributed to synchronised vortex shedding. The vortices shed from the upstream cylinder were associated with a peak in the lift coefficient on the downstream cylinder when the cylinders were 18° from the tandem configuration; a feature referred to as the "outer lift peak".

In considering flow over staggered cylinders at $Re = 4.52 \times 10^5$, Gu (1996) found that the interference effects in supercritical flows were significantly different to sub-critical flows. This included a reduction in the range of spacings where significant interference effects occurred (with the exception of tandem and near-tandem incidence angles). This further highlights the need to examine post-critical flow behaviour in detail.

Forces on equidistant three-cylinder arrangements in sub-critical flow (i.e., arranged at the corners of equilateral triangles) were recorded by Sayers (1987) at $Re = 3 \times 10^4$, with one cylinder instrumented with pressure taps. For the configuration with the instrumented cylinder upstream of two side-by-side cylinders, at the largest spacings ($s/d \geq 4$), the cylinder produced forces similar to that of an isolated cylinder, but as the spacing decreased, the drag also decreased, pointing to increased interference from the two downstream cylinders. For the largest spacing tested ($s/d = 5$), the drag on the cylinder increased as the arrangement was rotated, and peaked after 120° of rotation. This occurred at smaller rotation angles as the spacing was reduced. For all spacings, the minimum drag was recorded after ~150° of rotation, when the cylinder was directly in the wake of another cylinder, with large changes in the lift force also observed for rotation angles between 120° and 165°. Tatsuno et al. (1998) also examined the forces on sub-critical smooth cylinders in this arrangement, again finding that the interference effects were greatest for smaller spacings. Further work was done by Gu and Sun (2001), who attempted to classify the flow based on flow pattern visualisation and surface pressure measurements.

Sayers (1988) subsequently extended their work to four-cylinders in a square arrangement. Similar to the three-cylinder arrangement, they found the minimum drag to occur when the instrumented cylinder was directly in the wake of another cylinder (rotation angle of 135°, with 0° occurring when the cylinder was the upstream cylinder in a diamond-shaped arrangement). For larger spacings ($s/d \geq 3$), a second local minimum occurs at 180° of rotation. Additionally, the lift does not change significantly for rotation angles below 90°. However, above 90°, rapid changes in the magnitude and direction of the lift force were observed. For smaller spacings, both the lift and the drag displayed more variability at smaller rotation angles.

In this study we present results, specifically surface pressure measurements, from wind tunnel experiments of rough two-, three- and four-cylinder arrangements in post-critical flow. A range of wind angles and cylinder separation distances are tested for each configuration. We aim to extend our understanding of the aerodynamic forces experienced by interacting cylinders in the post-critical regime and to compare these to existing observations at lower Reynolds numbers. The results for the three- and four-cylinder arrangements are then compared to predictions of drag made based on different superposition approaches (see Price and Paidoussis (1984)).

2. Methodology

2.1. Wind tunnel

Experiments were conducted in the 1.4 MW wind tunnel of the Monash Wind Tunnel Research Platform (MWTRP). A closed-jet configuration was installed, with a $4 \times 2 \times 9.2$ m^3 (width × height × length) test-section. A schematic of the test section set-up, along with key dimensions, is shown in Fig. 2(a), and a photograph of the four cylinder arrangement is presented in Fig. 2(b).

The cylinders were mounted to a motorised turntable on the floor of the tunnel that was used to change the angle of incidence, θ, of the cylinder arrangements relative to the wind. The centre of the turntable was located at the streamwise and spanwise centre of the tunnel. At this location, the displacement and momentum thickness were approximately 12 mm and 10 mm respectively, on both the roof and floor of the tunnel. Outside the boundary layers, the turbulence intensity was approximately 1.35% and the variation in mean velocity was less than 0.5%. An integral length scale of the turbulence ($L_u \approx 0.14$ m) was estimated at the centre of the test section by fitting a von Kármán spectrum to the power spectral density of the fluctuations in the u-component of velocity.

At the mid-height of the tunnel, where the cylinders were instrumented with pressure taps, the mean velocity varied by less than 2% across the width of the tunnel within $\pm 6.5d$ of the tunnel centreline, noting that the furthest position of the centre of a cylinder from the midline of the tunnel was $5.8d$ across all tests. The streamwise turbulence intensity (I_{uu}) across this span ranged between 1.25% and 2%.

2.2. Cylinder setup

All cylinders had a diameter, d, of 204 mm. This included the surface treatment of the cylinders, for which P60 sandpaper was used to cover the surface of each cylinder. Based on the average sand-grain diameter, k, of the sandpaper as specified by the manufacturer, this resulted in a relative roughness of $k/d = 1.28 \times 10^{-3}$. Following the results of Achenbach and Heinecke (1981) and Spiedel (1954), the equivalent sand-grain roughness, k_s, was estimated to be $1.5 \times k$, yielding $k_s/d = 1.9 \times 10^{-3}$. The roughness Reynolds number in this study is taken as $Re_{k_s} = k_s U_\infty / \nu$, where U_∞ is the freestream velocity and ν is the kinematic viscosity. The data presented here was acquired at $Re_{k_s} = 770$, with variation in Re_{k_s} limited to ±6% of this value across all tests. There are additional sources of uncertainty for the roughness Reynolds number stemming from the reliance on the manufacturers stated sand-grain diameter that are difficult to quantify.

Each cylinder was instrumented with 30 equally spaced, 1.5 mm diameter pressure taps along its spanwise mid-plane to obtain instantaneous surface pressure measurements. For the two-cylinder arrangement, a second ring of pressure taps was installed $2d$ above the mid-plane for each cylinder. Two Dynamic Pressure Measurement Systems (DPMS) manufactured by Turbulent Flow Instrumentation (TFI) were used to record the pressures at 2000 Hz over a duration of 120

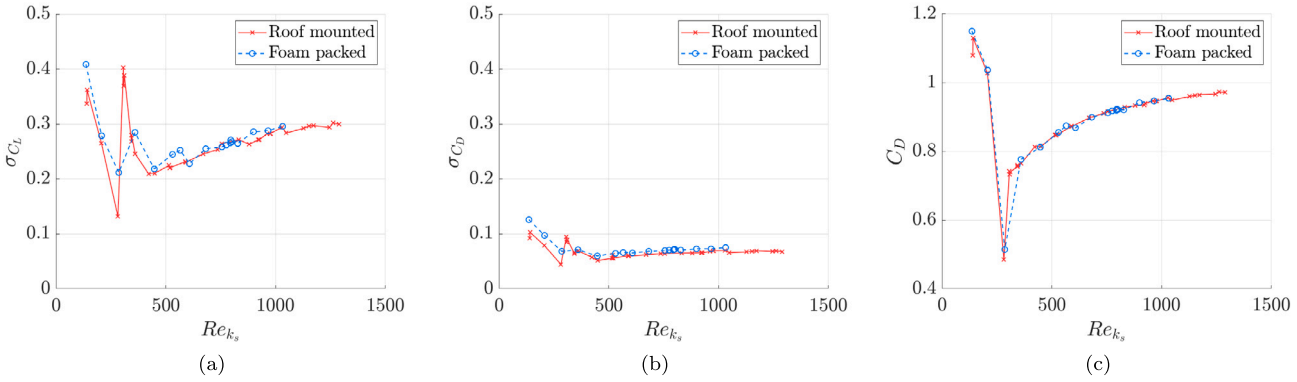

Fig. 1. Standard deviation of (a) lift and (b) drag for an isolated cylinder with different roof attachment configurations, and (c) mean drag for the isolated cylinder.

s and were connected to the taps using vinyl tubes. The time varying results were corrected to account for amplitude and phase distortions produced by the tube length following Bergh and Tijdeman (1965).

The local pressure coefficient, $C_{p,n}$, at each pressure tap was determined (Eq. (1)), where p_n is the pressure at tap n, p_0 is a reference static pressure, and ρ is the air density. The components of these pressures acting in the streamwise and cross-stream directions were summed to find, respectively, the pressure drag coefficient, C_D, and lift coefficient, C_L, (Eqs. (2) and (3)), where N is the total number of pressure taps, and ϕ_n is the azimuthal position of each pressure tap during a test, with $\phi = 0°$ corresponding to the most upstream point on the cylinder. The directions of the lift (L) and drag (D) forces are shown in Fig. 3.

$$C_{p,n} = \frac{p_n - p_0}{0.5\,\rho\,U_\infty^2} \tag{1}$$

$$C_D = \frac{\pi}{N}\sum_{n=1}^{N} C_{p,n}\cos\phi_n \tag{2}$$

$$C_L = \frac{\pi}{N}\sum_{n=1}^{N} C_{p,n}\sin\phi_n \tag{3}$$

The cylinders were mounted vertically and spanned the height of the tunnel, giving an aspect ratio of 9.8, which was identical to Pasam et al. (2023). To assess the spanwise uniformity of the cylinder, a cylinder instrumented with pressure taps at four spanwise locations was tested at a roughness Reynolds number of 775. The taps were located at the mid-span, 1d either side of the mid-span and 2d above the mid-span. The maximum variation in the mean and standard deviations of the force coefficients between the rings was 0.027 (noting the mean drag coefficient was ~1), indicating that the aspect ratio was sufficiently large to promote spanwise uniformity across the central portion of the cylinder. In general, the set-up of the cylinders was similar to Pasam et al. (2023), with the exception of the rigid mounting to the roof. A small ~5 mm gap to the roof was necessary to allow the cylinders to rotate with the floor turntable. This gap was packed with foam to prevent airflow through it. Using foam packing instead of mounting the cylinder to the roof could reasonably be expected to alter the mechanical response of the cylinder. To assess this effect, the forces on an isolated cylinder in the centre of the tunnel were measured for both the foam-packed (cantilever) and roof-mounted (fixed) configurations. For additional detail on the roof mounted cylinder, refer to Pasam et al. (2023). As shown in Fig. 1, while the standard deviations of the force coefficients increase (by around 0.01 for σ_{C_D}, and 0.02 for σ_{C_L}, in the post-critical range), the change in the mean drag coefficient is negligible and a small increase in lift coefficient is observed. For the two-cylinder arrangements, with the exception of the largest spacing, one of the cylinders had a 2 mm thick, 1.2d diameter end plate attached with a 3 mm gap to the roof, instead of the foam seal. To maintain the consistency of the dataset, data from this cylinder is not included (i.e., all presented data was taken from cylinders with foam sealing the gap to the roof and no end plate). As a consequence, the system force coefficients for the two cylinder arrangements are obtained by combining the coefficients from the same cylinder (in different positions) across separate tests. The system coefficients for the three- and four-cylinder arrangements are obtained from measurements taken simultaneously on all cylinders.

The blockage in the wind tunnel for the case of a single cylinder is approximately 5%, and higher with additional cylinders. A blockage correction has not been applied to the measured drag coefficients presented here; however, it is likely that the incremental velocity experienced by each cylinder in a given arrangement is a function of the local blockage conditions (i.e., whether the cylinder is side by side with another, behind or in front). Whilst the application of blockage corrections to multiple cylinder results requires further consideration, Roshko (1961), amongst others, provided a blockage correction for velocity and drag coefficient for a single cylinder. Applying these corrections, for indication, results in a reduction to the measured drag coefficients of the order of 3 to 7.5% depending on the configuration.

The uncertainties in the mean force coefficients are estimated to be ±0.03. This uncertainty estimate accounts for the accuracy of the instrumentation, the rotational variability of the cylinders (including the relative positioning of the pressure taps) and the repeatability of measurements.

The (centre-to-centre) spacing between the cylinders, s, was adjusted by moving the cylinders along four rails radiating from the centre of the turntable spaced 90° apart. Due to this configuration, the rotation axis for the three-cylinder arrangement was located between two cylinders instead of the centre of the arrangement. For the two-cylinder arrangement, the rotation axis was in line with the cylinder with the end plate for all but the largest spacing.

The coordinate systems used for each arrangement are depicted in Fig. 3. The cylinder numbers in this figure are used throughout this document to allow for greater clarity when discussing relative cylinder positions. All data on individual cylinders is presented as though it is taken from the position of cylinder 1. However, the data is acquired from all cylinders in each arrangement (with the exception of the aforementioned two-cylinder arrangements), and the symmetry of the arrangements is used to produce a combined dataset.

3. Results and discussion

3.1. Forces on two-cylinder arrangements

For most two cylinder configurations, the time-averaged lift and drag force coefficients on an individual cylinder within the arrangement were obtained from the surface pressure measurements on only one of the cylinders. This data is presented in Figs. 4 and 5 for the drag and lift, respectively. Again, these (and subsequent figures) present the

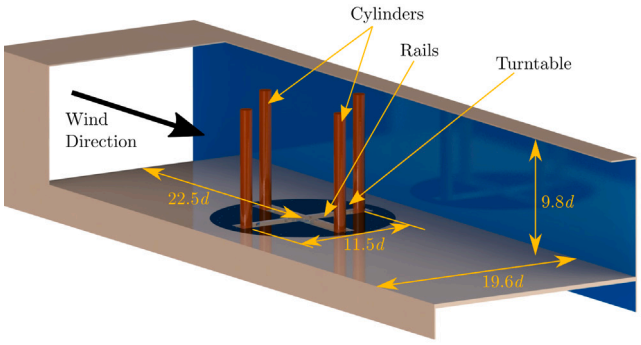

(a)

(b)

(c)

Fig. 2. (a) A diagram of the test section highlighting key dimensions as a function of the cylinder diameter: d, and components of the setup, (b) an example of the typical set-up used for the four-cylinder arrangements and (c) close-up of foam end-cap.

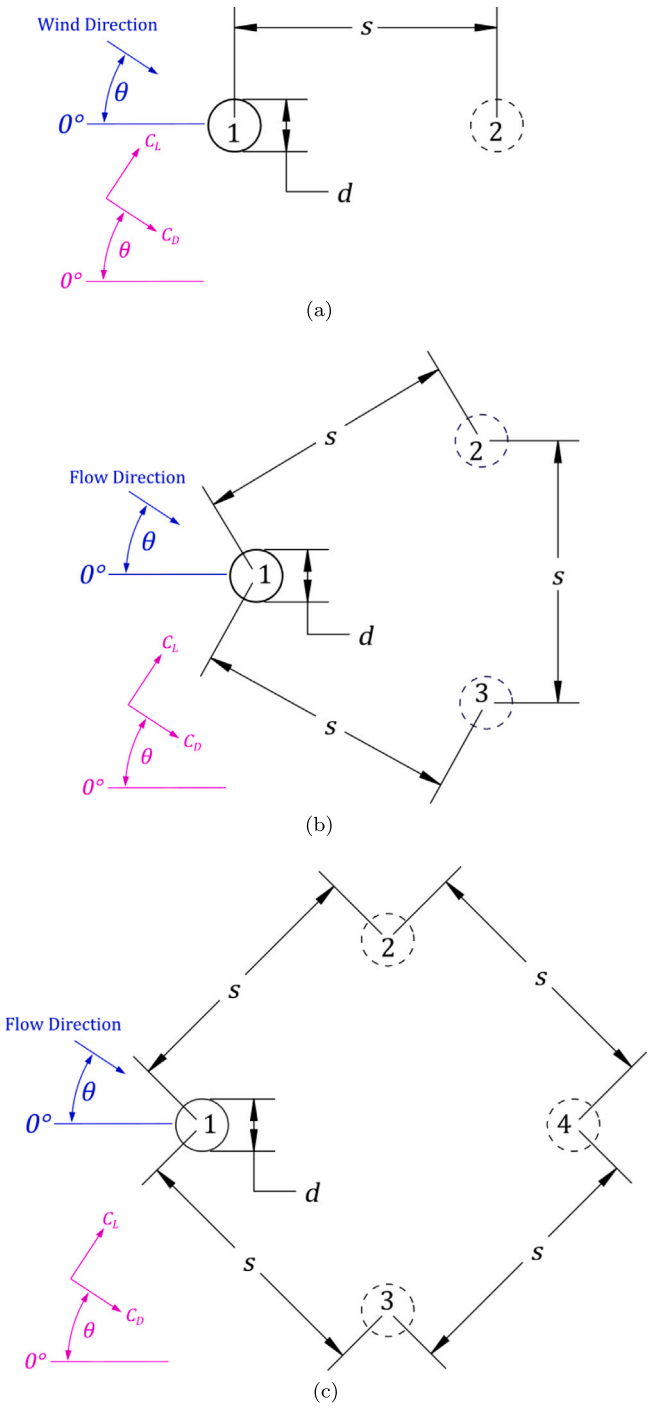

(a)

(b)

(c)

Fig. 3. Coordinate system and key dimensions for the (a) two-, (b) three- and (c) four-cylinder arrangements.

data as though it was measured on cylinder 1, noting that θ refers to the flow direction as defined in Fig. 3.

The highest mean drag coefficient for the two-cylinder arrangement occurs when the spacing between the cylinders is smallest ($s/d = 1.2$). As shown in Fig. 4, the drag for the two smallest spacings is higher than the other spacings for $40° \leq \theta \leq 80°$, with the maximum drag recorded at 70° for both cases. This range of configurations also produces the highest negative (outward) lift force (Fig. 5) across all spacings. The highest positive lift force also occurs when s/d is smallest, for $\theta = 10°$. For the smallest spacings, high lift coefficients were observed in the leeward cylinder when slightly offset from the inline position. Over this range of incidence angles, the mean lift is elevated when the cylinder is downstream ($155° \leq \theta \leq 175°$) for all spacings tested, but is highest when $s/d \leq 2.5$.

Not surprisingly, the drag minimum occurs at $\theta = 180°$ for all spacings, i.e., where cylinder 1 is directly leeward of cylinder 2. For some spacings below $s/d = 2.25$, a second local minimum was observed for incidence angles in the range $170° \leq \theta \leq 175°$. This feature was also observed by Sumner et al. (2005) for sub-critical smooth cylinders, although in that case, this secondary drag minimum represented the overall minimum drag for some spacings. A local maximum in the lift coefficient was associated with the secondary drag minimum in that study, which is also present here.

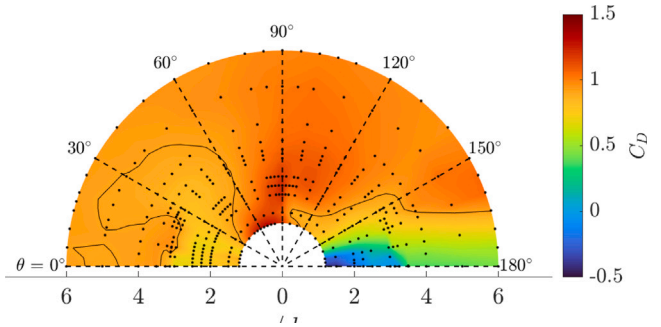

Fig. 4. Mean drag coefficient variation with θ and s/d for a single cylinder within a two-cylinder arrangement. The dots represent sampled points. The solid contour line represents a coefficient of 0.92 which was the drag coefficient measured on a single, isolated cylinder.

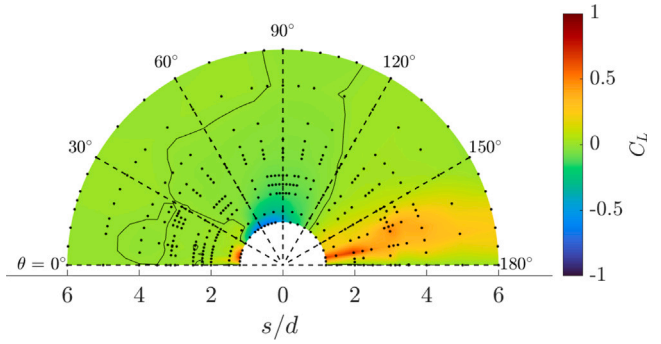

Fig. 5. Mean lift coefficient variation with θ and s/d for a single cylinder within a two-cylinder arrangement. The solid contour line indicates a lift coefficient of 0.

In comparison with the previous results in the sub-critical regime (Zhou and Alam, 2016; Sumner et al., 2005; Gu and Sun, 1999; Zdravkovich, 1977), the broad trends in the variation of the mean and fluctuating force coefficients in the post-critical regime remain similar. This indicates that the flow pattern does not change significantly between the two regimes. However, a few key differences are observed in the post-critical regime and these are explained below.

As the spacings increase from $s/d = 1.2$ and when the cylinder is downstream (i.e., $\theta \approx 180°$), a sharp increase in C_D occurs at $s/d \approx 3.25$. The corresponding "drag inversion spacing" in the sub-critical regime is $s/d \approx 4$. Drag inversion occurs at the spacing at which the separated shear layers from the upstream cylinder no longer reattach on the downstream cylinder. This is dependent on the vortex formation length, which reduces with increasing Reynolds number (Ljungkrona et al., 1991). A reduction in the drag inversion spacing for the same roughness and Reynolds number range is also explained in Pasam et al. (2024).

Sumner et al. observed a small, but sharp reduction in drag at incidence angles around 80°–90° for spacings below $s/d = 2$ as seen in Fig. 6. This reduction was also recorded by Gu and Sun (1999) for $Re = 2.2 \times 10^5$ for $s/d = 1.7$. In the present study, a reduction in the drag coefficient is observable when $s/d = 2$, although this occurs over a slightly different range of incidence angles compared with that of Sumner et al. for this spacing. This reduction is also present at $s/d = 2.25$ and 2.5 in the present study. The increase in drag which occurs at an incidence angle of approximately 90° in Gu and Sun (1999) was not replicated for any of the spacings examined by Sumner et al., and may be an artefact of inter-cylinder variation, given that both cylinders were instrumented. It is worth mentioning here that Gu (1996) observed a large reduction in drag at $s/d = 1.2$ for an incidence angle of around 85° in supercritical flow. However, larger spacings did not produce the same effect. The reduction in drag may be attributed to the cylinder transitioning from the "narrow wake-mode" to the "wide wake-mode".

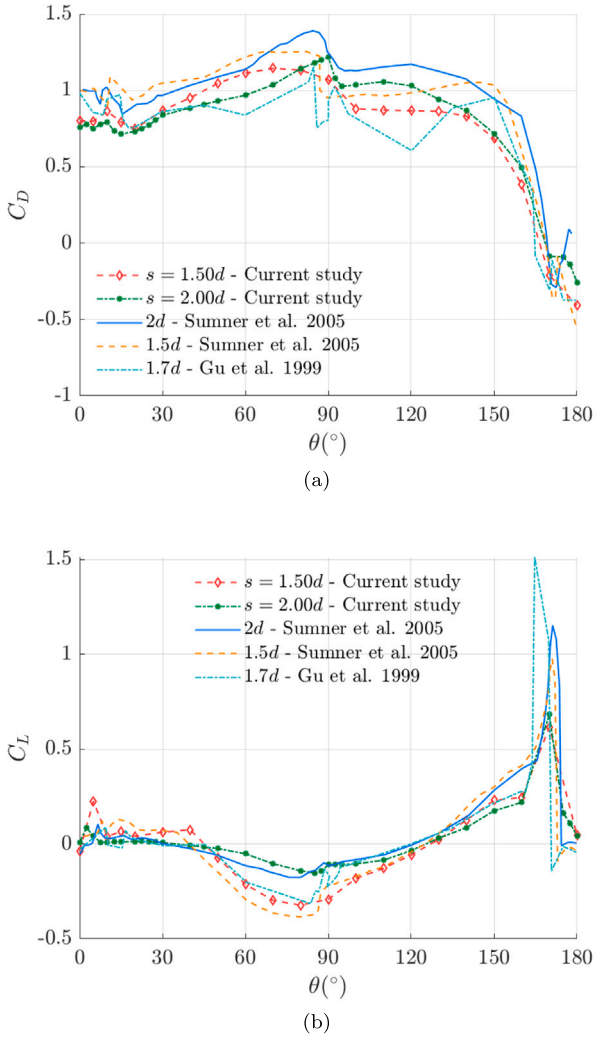

Fig. 6. Comparison with sub-critical flow of mean (a) drag and (b) lift coefficient variation with θ for a single cylinder within a two-cylinder arrangement.

In studies examining sub-critical flow by both Sumner et al. (2005) and Gu and Sun (1999), the reduction in drag seen at $s/d = 1.5$ and $s/d = 1.7$, respectively, is accompanied by a rapid reduction in the magnitude of the lift coefficient. However, the change in lift coefficient is substantially less pronounced in the present study and that seen by Sumner et al. (2005) at $s/d = 2$.

For $s/d \leq 1.5$, the drag coefficient in sub-critical flow is stable between approximately 90° and 140° before dropping sharply at higher incidence angles, whereas in the present study, the decline is more gradual and begins at smaller incidence angles. For larger spacings ($s/d > 1.5$) the variation of the force coefficients with incidence angle in the present study follows similar trends to the sub-critical flow study of Sumner et al.. While the drag coefficient magnitudes would be expected to differ between sub- and post-critical flow (as indeed is the case), the maximum lift coefficients are also substantially different, with sub-critical maximum lift coefficients often exceeding those in the present study by over 50% despite the maxima occurring at similar incidence angles. This feature also holds true for smaller spacings.

The larger cylinder spacings produce greater fluctuations in the lift (Fig. 7) and drag (Fig. 8) when the cylinders are within 30° of the in-line position. Previous studies on tandem cylinders (Alam et al., 2003b) have found similar increases, and associated them with the transition from the reattachment regime (where the shear layers from

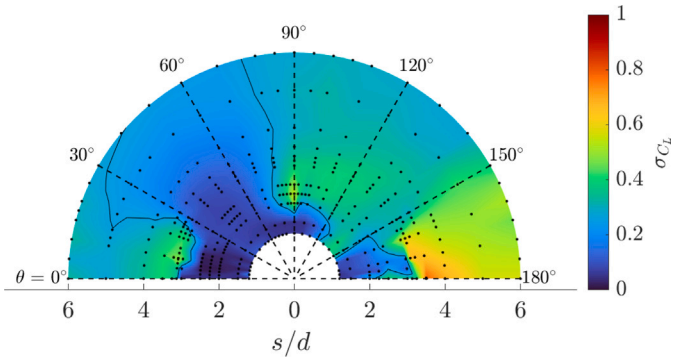

Fig. 7. Variation in the standard deviation of lift coefficient with θ and s/d for a single cylinder within a two-cylinder arrangement. The solid contour line represents a standard deviation of 0.26 which was the standard deviation of the lift coefficient measured on a single, isolated cylinder.

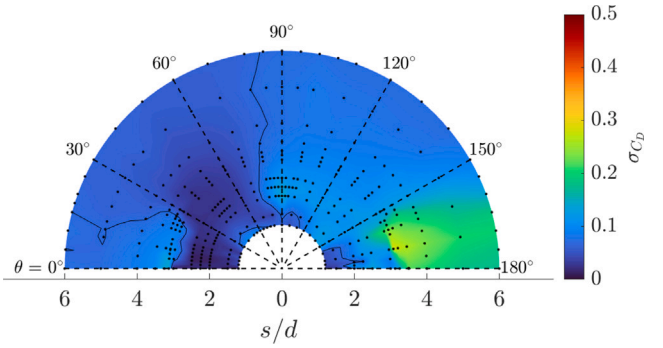

Fig. 8. Variation in the standard deviation of drag coefficient with θ and s/d for a single cylinder within a two-cylinder arrangement. The solid contour line represents a standard deviation of 0.07 which was the standard deviation of the drag coefficient measured on a single, isolated cylinder.

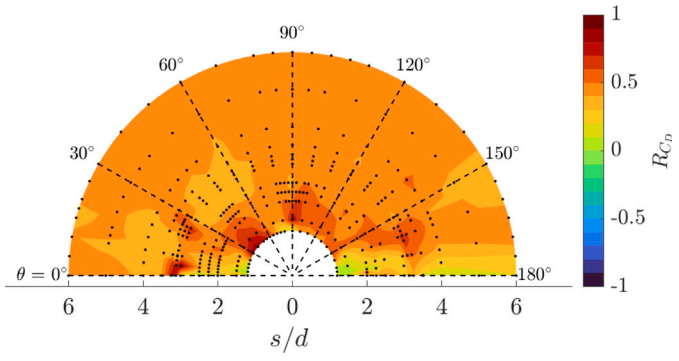

Fig. 9. Variation with θ and s/d of the correlation coefficient of C_D between the spanwise centre and $2d$ away for a single cylinder within a two-cylinder arrangement.

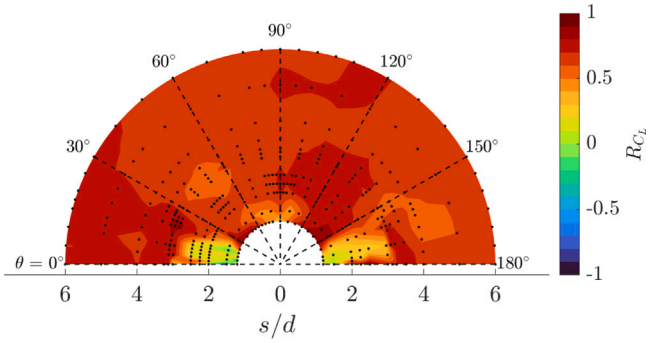

Fig. 10. Variation with θ and s/d of the correlation coefficient of C_L between the spanwise centre and $2d$ away for a single cylinder within a two-cylinder arrangement.

the upstream cylinder reattach on the downstream cylinder) to the co-shedding regime (where the gap between cylinders is large enough for vortices to form behind the upstream cylinder). Inspection of the time-dependent force coefficients (not shown) suggests there is bistability in the flow between $s/d = 3$ and $s/d = 3.25$ for certain incidence angles below 25°. This may contribute to the increased force fluctuations for these configurations and likely signifies the boundary between the co-shedding and reattachment regimes. Interestingly, unlike the lift coefficient, the fluctuations in the drag coefficient peak when the cylinders are offset from the in-line position.

Another band of increased fluctuations occurs when θ is close to 90° beginning from $s/d = 2$. In past studies on side-by-side cylinders (Alam et al., 2003a), this range of spacings has been associated with a transition from asymmetric to symmetric flow patterns. Outside this range of wind incidence angles, when the cylinders are close together ($s/d \leq 2.5$), the fluctuations in the force coefficients are typically smaller than for an isolated cylinder. The reduction is most pronounced when $\theta < 30°$, likely due to diminished influence of Kármán shedding due to interference from the other cylinder.

Correlation coefficients were obtained for the drag (Fig. 9) and lift (Fig. 10) between the mid-span of the cylinder and a plane $2d$ above the mid-span on the same cylinder. Overall, the lift is more strongly correlated across the span of the cylinders than the drag, with the strongest correlation observed for the smallest spacing when $30° \leq \theta \leq 60°$ for both components. Both components are weakly correlated for $s/d < 3$ when the cylinders are within approximately 30° of the in-line position in both the upstream and downstream position, although for the in-line position itself, the lift correlation strengthens above spacings of $s/d = 2$. This latter behaviour agrees with Pasam et al. (2024), who further also examined the correlation of the lift coefficient on tandem cylinders after the application of a median filter, finding that the filtered lift was negatively correlated for $s/d \leq 2.25$. They found that for in-line cylinders with spacings of $1.5 \leq s/d \leq 2.25$, the shear layers from the upstream cylinder would reattach on the downstream cylinder, but would do so asymmetrically, resulting in a clearly identifiable alternating bi-stability. They ascribed the negative correlations of the filtered lift to the presence of spanwise "cells" which each exhibited different reattachment configurations.

Overall, the variation of the force coefficients with incidence angle display clear differences between the largest spacings examined ($s/d \geq 3.5$) and moderate spacings ($2 \leq s/d \leq 2.5$). In the range $3 \leq s/d \leq 3.25$, the trends mostly resemble the larger spacings, but diverge from them on occasion. The behaviour of the two closest spacings ($s/d \leq 1.5$) is distinct from the other spacings. However, while they produce similar trends in the drag coefficient to each other, there are prominent differences in the behaviour in the lift coefficient, particularly when $\theta < 30°$, where the $s/d = 1.2$ case produces high positive lift.

3.2. Forces on three-cylinder arrangements

The mean drag coefficient on cylinder 1 for the different three-cylinder configurations is shown in Fig. 11. In broad terms, the drag coefficient is lowest when the cylinder is in the wake of cylinder 2, i.e., close to $\theta = 150°$, where these two cylinders are aligned with the wind direction. The interference from cylinder 2 increases as s/d decreases, leading to a lower drag minimum as well as a wider range of incidence angles for which the drag coefficient falls below that of the isolated cylinder. The maximum drag for each spacing occurs between these wake-affected incidence angles and $\theta = 90°$. For $s/d \geq 4$, the drag coefficient is also larger than the isolated cylinder drag as the incidence angle increases beyond the wake-affected angles. Local increases in

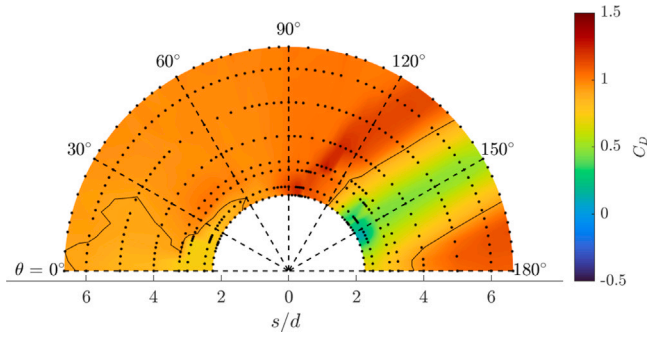

Fig. 11. Mean drag coefficient variation with θ and s/d for a single cylinder within a three-cylinder arrangement. The solid contour line represents a coefficient of 0.92 which was the drag coefficient measured on a single, isolated cylinder.

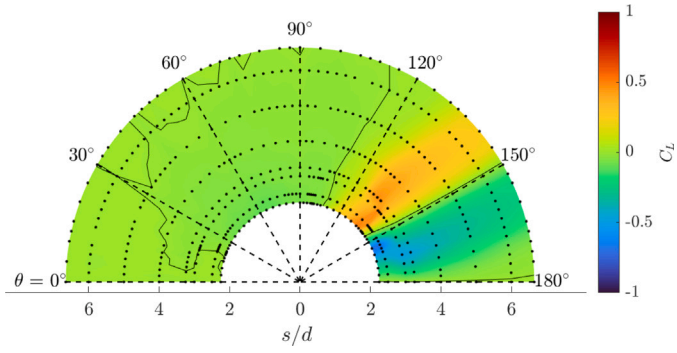

Fig. 12. Mean lift coefficient variation with θ and s/d for a single cylinder within a three-cylinder arrangement. The solid contour line indicates a lift coefficient of 0.

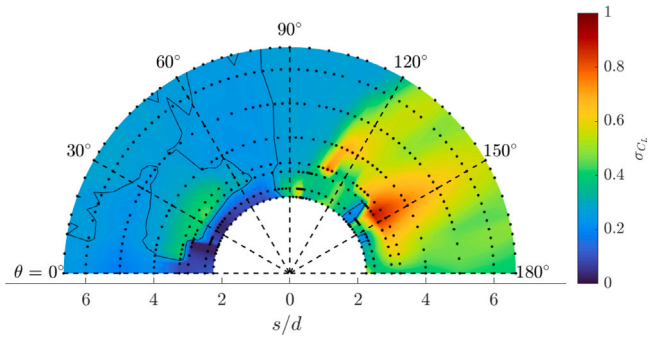

Fig. 13. Variation in the standard deviation of lift coefficient with θ and s/d for a single cylinder within a three-cylinder arrangement. The solid contour line represents a standard deviation of 0.26 which was the standard deviation of the lift coefficient measured on a single, isolated cylinder.

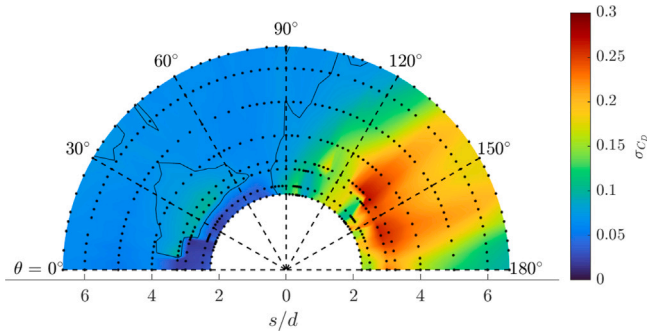

Fig. 14. Variation in the standard deviation of drag coefficient with θ and s/d for a single cylinder within a three-cylinder arrangement. The solid contour line represents a standard deviation of 0.07 which was the standard deviation of the drag coefficient measured on a single, isolated cylinder.

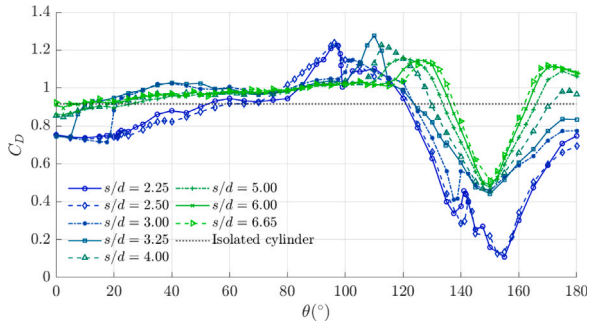

Fig. 15. Variation with θ of the mean drag coefficient on a single cylinder within a three-cylinder arrangement for each s/d.

the velocity beyond the freestream velocity immediately outside the boundary layer (and subsequently, the separated shear layer) over circular cylinders have previously been observed (e.g., Pasam et al., 2023) that could explain these increases.

The mean lift coefficient, presented in Fig. 12 generally does not vary significantly except for the wake-affected incidence angles. As the incidence angle increases and cylinder 1 enters the wake of cylinder 2, the lift coefficient rapidly increases to reach its maximum before rapidly decreasing and reaching its minimum as the incidence angle increases further and the cylinder begins to leave the wake of cylinder 2. Both the minima and maxima increase in magnitude as s/d decreases, demonstrating the increased interference at smaller spacings. Additionally, while the larger spacings have lift coefficients close to zero at the minimum drag incidence angle, when $s/d \leq 2.5$ substantial ($C_L < -0.29$) negative lift was observed, likely due to greater influence from cylinder 3 at these spacings.

The fluctuating lift (Fig. 13) and drag (Fig. 14) generally follow similar distributions to each other for $\theta < 120°$, although the fluctuations in lift are larger in magnitude. For $s/d \geq 2.5$, the highest fluctuations in lift occur when cylinder 1 is directly downstream of cylinder 2, or close to it ($145° \leq \theta \leq 150°$), across the different spacings. The highest drag fluctuations however, occur when cylinder 1 is downstream of cylinder 2, but offset from the in-line position by 10°–15°.

The mean force coefficients indicate the presence of two distinct regimes based on the cylinder spacing. This is more evident when the coefficients for each spacing are viewed separately, as depicted in Figs. 15 and 16. The first regime occurs for the smallest distances tested, $s/d = 2.25$ and $2.5d$. The mean drag is noticeably lower than that of an isolated cylinder when a cylinder is in its furthest upstream positions and unlike the two-cylinder arrangement, the minimum drag does not occur when cylinder 1 is directly behind cylinder 2 (i.e., when $\theta = 150°$). Instead, it occurs when cylinder 1 is slightly (1–5°) offset from the in-line position. The location of the minimum is consistent with previous studies on sub-critical flows at similar spacings (Gu and Sun, 2001; Tatsuno et al., 1998; Sayers, 1987). These studies also found a gradual decline in drag leading to the minimum drag incidence angle, beginning from $\theta = 100 - 120°$. The decline found in those studies was punctuated by occasional small increases when $\theta > 135°$, which is consistent with the present study.

Not all aspects of the trend in drag are consistent between the sub-critical studies (Gu and Sun, 2001; Tatsuno et al., 1998; Sayers, 1987) and the present study. For example, those sub-critical studies observed a prominent local maximum in the drag coefficient that typically occurred when θ is between 25° and 35°, but is absent in the present study. Additionally, in this study, for $s/d = 2.25$, there is a local maximum in the drag at 97.5°, followed by a steep reduction at 100° and a rapid increase at 102.5°. When $s/d = 2.5$, a small reduction is

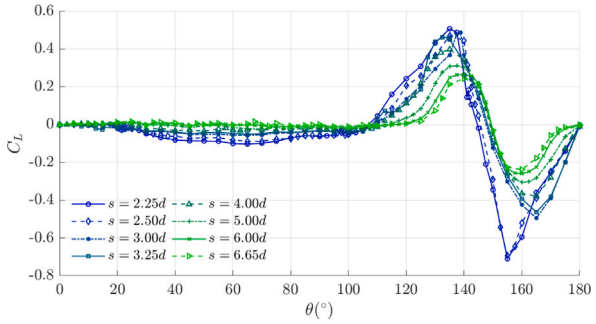

Fig. 16. Variation with θ of the mean lift coefficient on a single cylinder within a three-cylinder arrangement for each s/d.

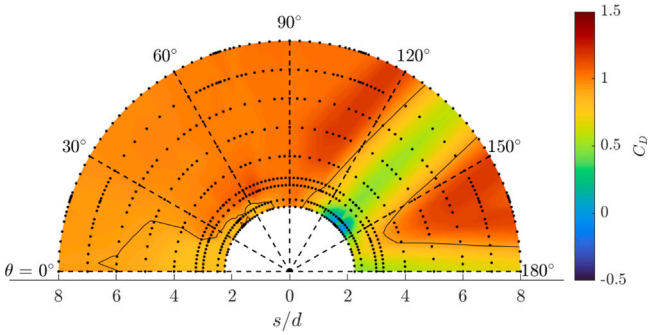

Fig. 17. Mean drag coefficient variation with θ and s for a single cylinder within a four-cylinder arrangement. The solid contour line represents a coefficient of 0.92 which was the drag coefficient measured on a single, isolated cylinder.

present, but the rapid increase at higher angles is not. While this feature was not observed by Gu and Sun (2001) for $s/d = 2.2$, it does appear when $s/d = 2.5$ and is partially present (without the sharp recovery) when $s/d = 2.5$ in Sayers (1987). This occurs in the region where cylinder 1 transitions from being offset from the other two cylinders at $\theta = 90°$ to interacting with them, resulting in high gradients in the drag coefficient. Furthermore, this suggests that differences in the flow at post-critical Reynolds numbers can lead to variations in flow behaviour and forces for similar spacings, especially in regions of high gradients. Apart from these features, the drag follows similar trends to the sub-critical studies. As with the two-cylinder case, the lift coefficient also exhibits similar behaviour to the sub-critical studies, but with maxima that are lower in magnitude.

At larger spacings ($s/d \geq 4$), the trends in lift and drag with incidence angle do not deviate significantly from those observed in sub-critical studies, with the exception of an outlier at $s/d = 4$ and $\theta = 158°$ in Sayers (1987). Broadly, the drag is similar to or slightly higher than the isolated cylinder for incidence angles below 110° before increasing and then experiencing a prolonged decline as cylinder 1 enters the wake of cylinder 2, reaching a minimum when the cylinders are directly in line at $\theta = 150°$. This maximum drag declines as the spacing increases, while the minimum drag increases with spacing, reducing the overall variation in drag with incidence angle. The variation in the mean lift coefficient also decreases as the spacing increases.

Similar to the two-cylinder case, $3 \geq s/d \geq 3.25$ appears to be transitional spacing, with aspects of both the larger and smaller spacing trends present. The highest values of σ_{C_L} and σ_{C_D} occur over these spacings. Observations of the time-dependent force coefficients suggested that the flow was bistable for system incidence angles close to 10° when $s/d = 3.25$. This accounts for the sharp increase in σ_{C_L} at $\theta = 110°$ for this spacing. Bistability was also observed for incidence angles close to 20° when $s/d = 2.25$ and $s/d = 3$, although these configurations do not correspond to distinct increases in the fluctuating forces.

3.3. Forces on four-cylinder arrangements

The trends in the force coefficients for the four-cylinder arrangements are largely consistent with the three-cylinder case for small incidence angles. For the smallest spacings ($s/d \leq 2.5$), the mean drag on an individual cylinder within the arrangement, depicted in Fig. 17, is lower than that of an isolated cylinder for small incidence angles. For these spacings, the minimum drag does not occur when cylinders 1 and 2 are inline, but at a 5°–10° offset. Instead, there is a sharp increase in drag between the minimum and the inline (i.e. $\theta = 135°$) positions (this is more readily apparent in Fig. 18). In sub-critical flow, Sayers (1988) also observed that the minimum drag occurs when

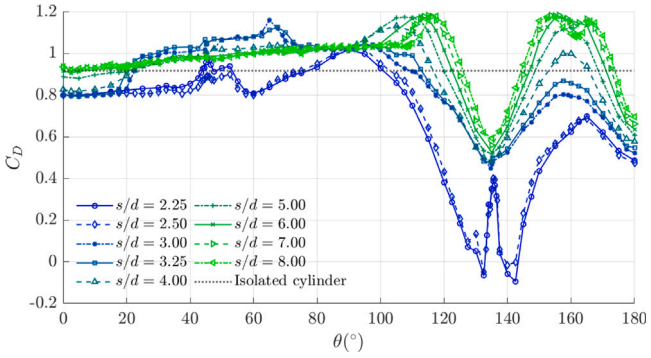

Fig. 18. Variation with θ of the mean drag coefficient on a single cylinder within a four-cylinder arrangement for each s/d.

the cylinders are not inline when $s/d \leq 2$ (instead occurring around $\theta = 127°$), although the second minimum observed in the present study above 135° was not present, possibly due to the lower angular resolution of that study. Apart from this, the trends in lift and drag with incidence angle are broadly consistent with the sub-critical flow examined by Sayers (1987). This includes the behaviour of the lift coefficient (Figs. 19 and 20) when the aforementioned drag increase occurs. The lift is negligible when the drag reaches its local maximum at 135°, but rapidly becomes more negative as the incidence angle increases and more positive as the incidence angle decreases.

The similarity to sub-critical flows extends to larger spacings ($s/d \geq 4$), where the effects of increasing the spacing on the variation in the force coefficients is similar to those seen for the three-cylinder arrangements. Perhaps the only notable difference here is the appearance of a local drag minima at $\theta = 162°$ for the two largest spacings. This corresponds to an inflection point in the lift as it increases between $142.5° \leq \theta \leq 170°$.

The spacings of $s/d = 3$ and 3.25 mostly produce force coefficient trends similar to the larger spacings, although for some incidence angles, similarities to the smaller spacings and other distinct trends are evident. As seen in Fig. 21, akin to the two- and three-cylinder arrangements, these spacings are responsible for high values of σ_{C_L} when cylinders 1 and 2 are close to the inline position. As with the two-cylinder results, for these spacings, the drag fluctuations peak when the cylinders are offset from the in-line position (see Fig. 22). Bistable behaviour was also observed in this case, around $\theta = 22.5°$ and 45° for $s/d = 3$, 20° for $s/d = 3.25$, and 45° for $s/d = 2.5$. This may contribute to the elevated fluctuations for the some of these configurations.

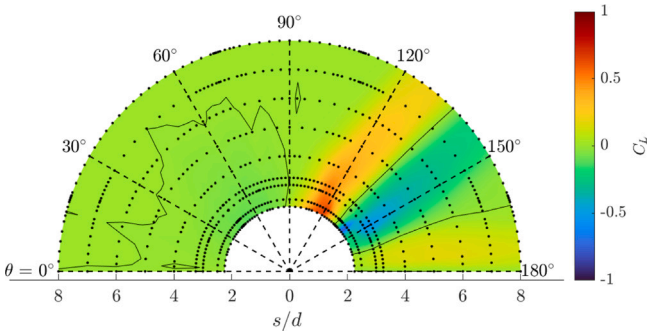

Fig. 19. Mean lift coefficient variation with θ and s for a single cylinder within a four-cylinder arrangement. The solid contour line indicates a lift coefficient of 0.

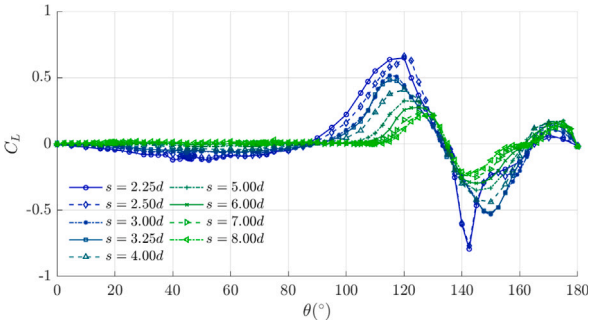

Fig. 20. Variation with θ of the mean lift coefficient on a single cylinder within a four-cylinder arrangement for each s/d.

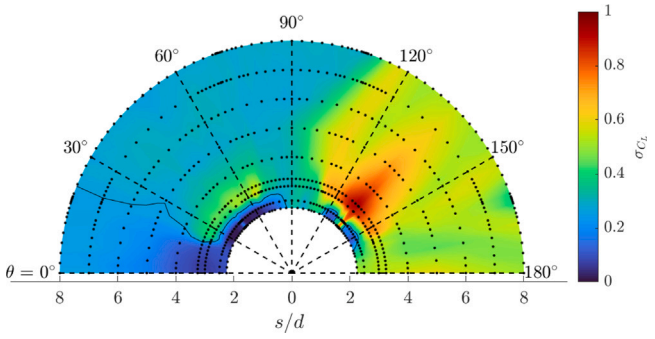

Fig. 21. Variation in the standard deviation of lift coefficient with θ and s/d for a single cylinder within a four-cylinder arrangement. The solid contour line represents a standard deviation of 0.26 which was the standard deviation of the lift coefficient measured on a single, isolated cylinder.

3.3.1. Similarity of downstream cylinder drag to the two-cylinder arrangement

For a given cylinder in a three- or four-cylinder arrangement, it is possible to describe its position relative to each of the other cylinders in the arrangement. This effectively treats the cylinder as though it was a part of two or three separate cylinder pairs, respectively (e.g. a cylinder in a three-cylinder arrangement at $\theta = 120°$ can described as being part of two two-cylinder arrangements with $\theta = 90°$ relative to one of the other cylinders and $\theta = 150°$ relative to the other). A comparison of the cylinder force coefficient trends using this approach is visualised in Figs. 23 and 24, where the incidence angle of the two-cylinder

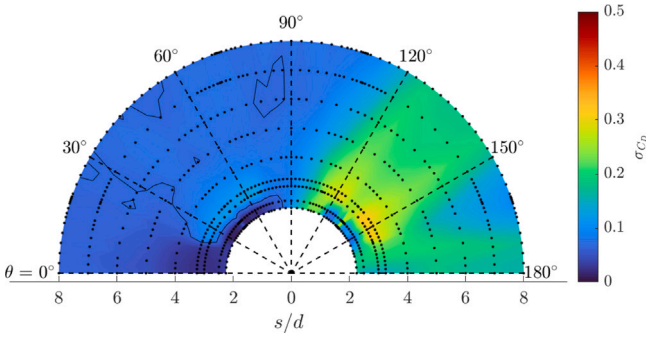

Fig. 22. Variation in the standard deviation of drag coefficient with θ and s/d for a single cylinder within a four-cylinder arrangement. The solid contour line represents a standard deviation of 0.07 which was the standard deviation of the drag coefficient measured on a single, isolated cylinder.

arrangements is offset such that the relative cylinder positions match those of each pair of cylinders within the three-cylinder arrangement. It is clear that the interference effects are sensitive to the incidence angle, with broad similarities apparent between the two cases.

In comparing individual cylinders within arrangements of two and three cylinders, Price and Paidoussis (1984) also found some similarities in the interference effects from the other cylinders in the arrangement on the aerodynamic forces at sub-critical Reynolds numbers. This led them to attempt to predict the forces on one cylinder within a group of three based on the forces on two cylinder arrangements using a "superposition principle". The three cylinder arrangements in that study consisted of two side-by-side cylinders and a third cylinder on which forces were measured for different combinations of spacings between the side-by-side cylinders and streamwise and cross-stream positions of the measured cylinder. They found the superposition approach to be reasonably accurate for most combinations tested, with the lift coefficient better predicted than the drag coefficient.

In the present study, we attempt to extend similar approaches to those of Price and Paidoussis to all cylinders within three- and four-cylinder arrangements in post-critical flows. Adapted to the arrangements used here, their first approach to predicting the drag, which is based on the interference, is given in Eq. (4). Here $C^{(i)}_{D_{1,23}}$ represents the predicted drag on cylinder 1 with cylinder 2 and 3 present, $C^{(i)}_{D_{1,2}}$ represents the measured drag on cylinder 1 with only cylinder 2 present, $C^{(i)}_{D_{1,3}}$ represents the measured drag on cylinder 1 with only cylinder 3 present and $C^{(i)}_{D_1}$ represents the measured drag on cylinder 1 with no other cylinders present.

$$C^{(i)}_{D_{1,23}} = C_{D_{1,2}} + C_{D_{1,3}} - C_{D_1}. \tag{4}$$

Their approach to the lift coefficient follows a similar principle, apart from the absence of the C_{D_1} equivalent term due to the negligible mean lift on the isolated cylinder. Therefore, for brevity's sake, the equations for a cylinder that is part of a N-cylinder cluster for both the lift and drag coefficients can be represented by Eq. (5), where F represents the force (i.e., lift or drag), $C_{F_{1,j}}$, represents the force coefficient for cylinder 1 with cylinder j present and is taken from the two-cylinder results, and C_{F_1} represents the isolated cylinder force coefficient (set to zero for lift). This approach is subsequently referred to as method (i).

$$C^{(i)}_F = \sum_{j=2}^{N}(C_{F_{1,j}}) - (N-2)C_{F_1}. \tag{5}$$

The second approach, method (ii), used for the drag by Price and Paidoussis is simply the mean of the two-cylinder coefficients, denoted here as

$$C^{(ii)}_F = \frac{\sum_{j=2}^{N}(C_{F_{1,j}})}{N-1}. \tag{6}$$

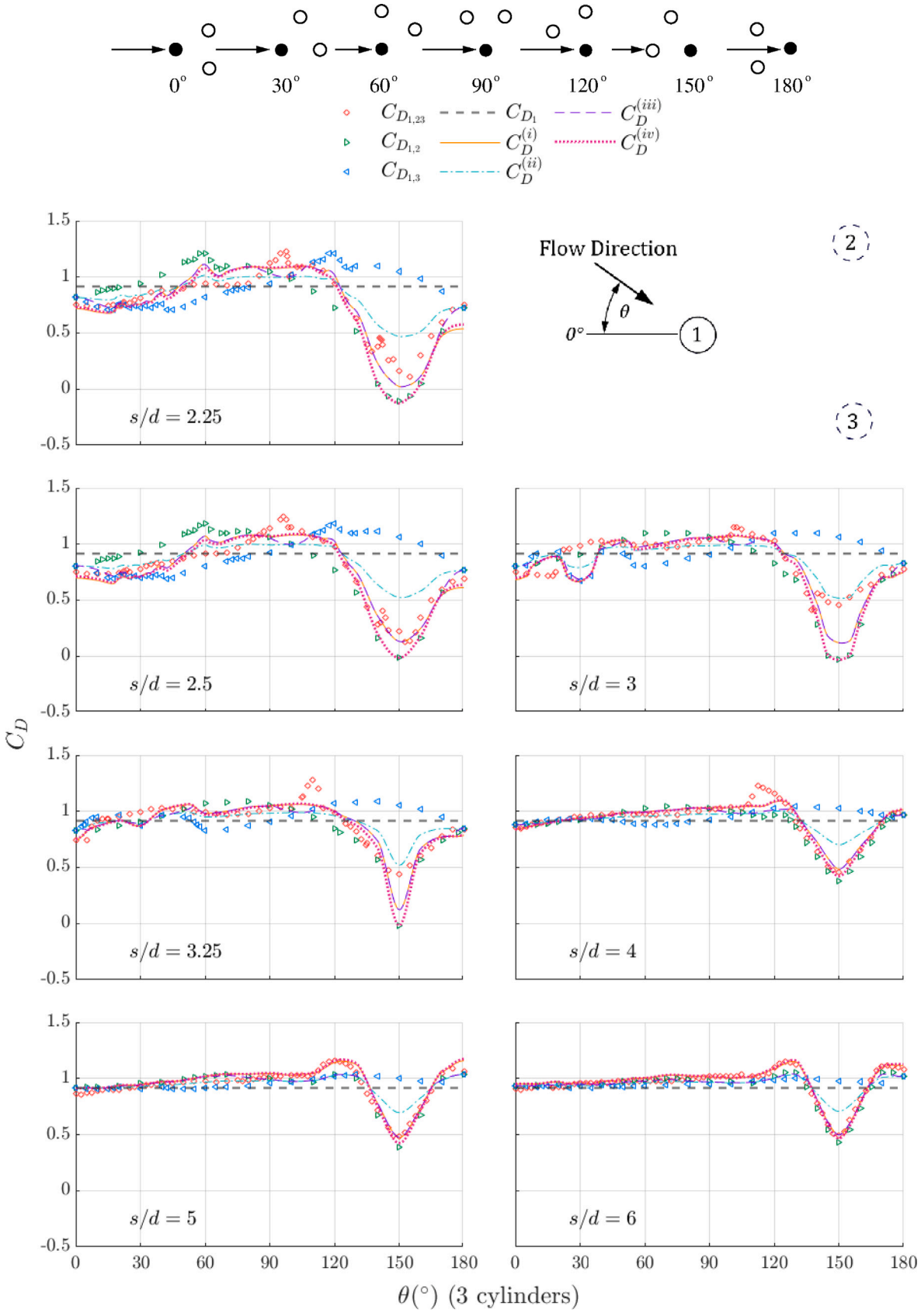

Fig. 23. Comparison of mean drag coefficient variation with θ between individual cylinders within a three-cylinder arrangement and different predictions based on individual cylinders within a two-cylinder arrangement in similar relative positions.

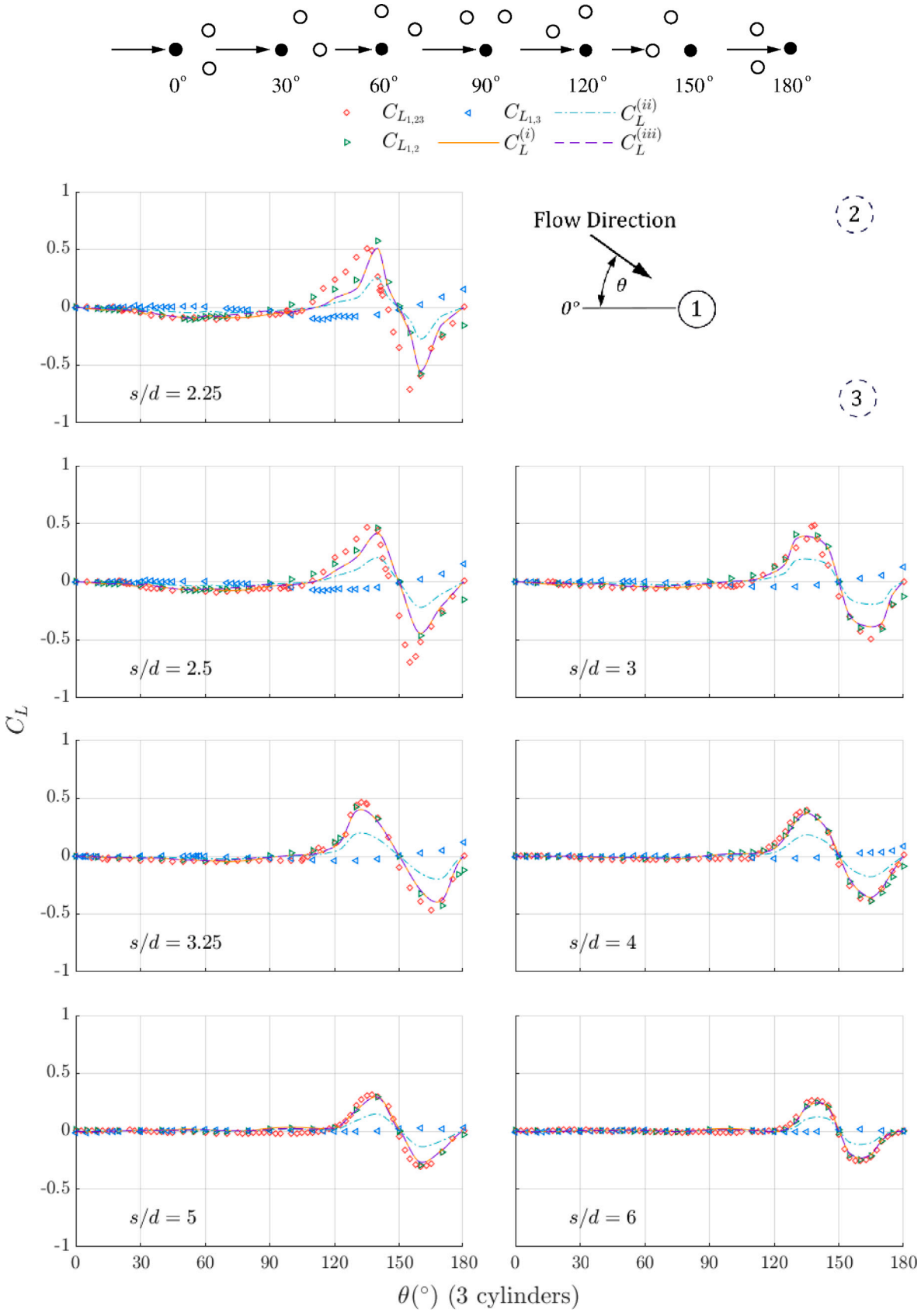

Fig. 24. Comparison of mean lift coefficient variation with θ between individual cylinders within a three-cylinder arrangement and different predictions based on individual cylinders within a two-cylinder arrangement in similar relative positions.

Two additional approaches are also attempted here. Similar to those of Price and Paidoussis, these approaches do not have a strict theoretical justification, but nevertheless provide useful results. Firstly, referred to henceforth as method (*iii*), a weighted average is used, with the weights based on the difference between the corresponding two-cylinder and isolated cylinder force coefficients. The reasoning behind this is that the greater deviations from the isolated-cylinder coefficients signify a larger interference effect that would be expected to have a disproportional effect on the three- and four-cylinder coefficients.

$$C_F^{(iii)} = \frac{\sum_{j=2}^{N} C_{F_{1,j}}(|C_{F_{1,j}} - C_{F_1}|)}{\sum_{j=2}^{N}(|C_{F_{1,j}} - C_{F_1}|)}. \tag{7}$$

Another attempted approach, method (*iv*), consists of multiplying the isolated cylinder coefficient by the ratio of each two-cylinder coefficient to the isolated-cylinder coefficient. This approach effectively treats the interference effects as though they were changes to the local dynamic pressure. Due to the negligible lift for the isolated cylinder, this method is only applied to the drag coefficient.

$$C_F^{(iv)} = C_{F_1} \prod_{j=2}^{N} \frac{C_{F_{1,j}}}{C_{F_1}}. \tag{8}$$

In general, the drag predictions for the three-cylinder case, not surprisingly, improve as s/d increases. Overall, $C_D^{(i)}$ is closest to the measured drag values, but $C_D^{(iii)}$ and $C_D^{(iv)}$ are also reasonably good predictions. For $s/d \leq 4$, none of the approaches capture the local maximum in the drag between $\theta = 95°$ and 130°. This is to be expected given its absence in this range for the two-cylinder cases. For $s/d \geq 5$, the local maximum near $\theta = 120°$ is predicted well by $C_D^{(i)}$ and $C_D^{(iv)}$. For most instances, method (*ii*) underestimates the drag when the cylinder is downstream in near-tandem positions. The exceptions to this are the $s/d = 3$ and 3.25 cases, where $C_D^{(ii)}$ outperforms the other predictions due to the extremely low drag for the two-cylinder arrangement in these configurations. For these two spacings, the predictions also diverge from the measured trend below 45°, and together these indicate that the transition between the high and low-spacing flows is affected by the presence of a third cylinder.

The lift coefficient is well predicted by $C_L^{(i)}$ and $C_L^{(iii)}$ for the larger spacings ($s/d \geq 3.25$). However, $C_L^{(ii)}$ consistently underestimates the magnitudes of the maximum and minimum lift coefficients. For the two smallest spacings, the lift coefficient predictions diverge from the measured values for incidence angles where cylinder 1 is in the wake of cylinder 2. The influence of cylinder 3 is obvious here, as the predicted lift is close to zero when cylinders 1 and 2 are in the tandem orientation ($\theta = 150°$) while the measured lift is substantial.

For the four-cylinder arrangement, the diagonally-opposed pair (between cylinders 1 and 4) has a different spacing between cylinders to the other pairs. Therefore, the closest tested spacing is presented in Figs. 25 and 26, denoted by $C^*_{D_{1,4}}$ and $C^*_{L_{1,4}}$. This is significantly different ($> 2d$) to the actual spacing of the cylinders for the larger spacings, but nevertheless useful for the purposes of the present comparison. For the application of Eqs. (2)–(5) in those figures, $C_{D_{1,4}}$ is interpolated linearly from the two nearest spacings. Linear extrapolation was used for the two largest spacings.

It is possible that the use of extrapolation for the largest spacings contributes to the overestimate by $C_D^{(i)}$ and $C_D^{(iv)}$ of the drag maximum at $\theta \approx 160°$ observed for those spacings, as well as the overestimate for $\theta < 90°$. However, while these configurations are better predicted at $s/d = 3.25$ and 4, they are still overestimated, suggesting that the extrapolation is not the sole cause for this. Due to these overestimates, method (*iii*) produces the closest predictions overall for the drag coefficients for these configurations, although it underestimates the drag maximum near $\theta = 100°$. Similar to the three-cylinder configurations, method (*ii*) consistently overestimates the minimum drag. However, the other approaches predict this well for the three largest spacings. Apart from $s/d = 3$, these approaches consistently predict the drag reasonably well for incidence angles below 120° when $C_{D_{1,4}}$ is interpolated. The deviation for $s/d = 3$ may again be due to differences in the transition between regimes relative to the two-cylinder configurations.

Despite the extrapolation of $C_{D_{1,4}}$ for the higher spacings, the lift coefficient is well predicted by $C_D^{(i)}$, $C_D^{(iii)}$ and $C_D^{(iv)}$ for $s/d \geq 4$, while method (*ii*) again consistently underestimates the highest lift magnitudes. The predictions become less accurate as the spacing decreases, with the trend around the highest lift magnitudes being particularly poorly predicted for the two smallest spacings.

Overall, the results suggest that the coefficients for both the three- and four-cylinder configurations can be estimated from two-cylinder arrangements if the spacing between the cylinders is sufficiently large ($s/d \geq 4$). For the smallest spacings ($s/d \leq 2.5$) examined here, reasonable estimates can be produced for incidence angles below 90°. When the spacings are in the transitional range ($3 \geq s/d \geq 3.25$), the predictions only sporadically match the measured coefficients.

Further, we have also applied these prediction methodologies to the three-cylinder results of Price and Paidoussis (1984). The analysis is presented in the Appendix section below. It demonstrates that these methodologies remain viable for sub-critical flow and non-equidistant arrangements, but are not valid for small spacings.

3.4. Forces on systems of cylinders

In addition to the forces on individual cylinders within the system, the forces on the system as a whole were also considered. The system lift ($C_{L,sys}$) and drag ($C_{D,sys}$) coefficients are taken as the sum of the coefficients on all cylinders divided by the number of cylinders in the arrangement.

3.4.1. Two-cylinder system forces

The drag (Fig. 27) and lift (Fig. 28) coefficients for the two-cylinder arrangements provide further support for the notion of different flow regimes based on cylinder spacing. The trends for both force coefficients form clusters based on the same spacing regimes observed for individual cylinders within the system. The difference between the $s/d = 1.2$ case and the larger spacing configurations is pronounced in the system forces, particularly the lift. For incidence angles of $\theta > 30°$, the lift coefficient is close to zero for $s/d > 1.5$, but for $s/d = 1.2$, high magnitude lift coefficients were observed for this range of angles. Additionally, when $\theta < 30°$, substantial lift occurs for most spacings, but the direction of the highest magnitude lift for $s/d = 1.2$ is opposite to the other spacings.

The maximum system drag across all cases tested occurred for the intermediate spacings ($2 \geq s/d \geq 2.5$) when the system was in the side-by-side configuration. In general, both the drag and the lift see reduced variation with incidence angle as the spacing increases.

3.4.2. Three- and four-cylinder system forces

The measured total system forces on the three- and four-cylinder arrangements are presented in Figs. 29–32. Similar to the two-cylinder arrangements, the variation in the coefficients with wind angle decreases as the spacing between the cylinders increases. Additionally, following the results for individual cylinders within the arrangements, the trends display clear distinctions between the larger ($s/d \geq 4$) and smaller ($s/d \leq 2.5$) spacings. For the two largest spacings of the four-cylinder arrangement, a local minima in the drag (Fig. 31) is observable at $\theta = 18°$, which corresponds to a reduction in drag on cylinder 4 ($\theta = 162°$). This is absent when s/d is smaller.

The transition in the trends between the smaller and larger spacing for $s/d = 3$ and 3.25 is clear in the drag on the three-cylinder arrangements (Fig. 29). For small wind incidence angles, the drag coefficients a bear greater resemblance to the smaller s/d cases, before a clearly visible "switch" in the trends to the larger s/d cases as θ increases. Such a prominent change is not observed in the four-cylinder drag, with the

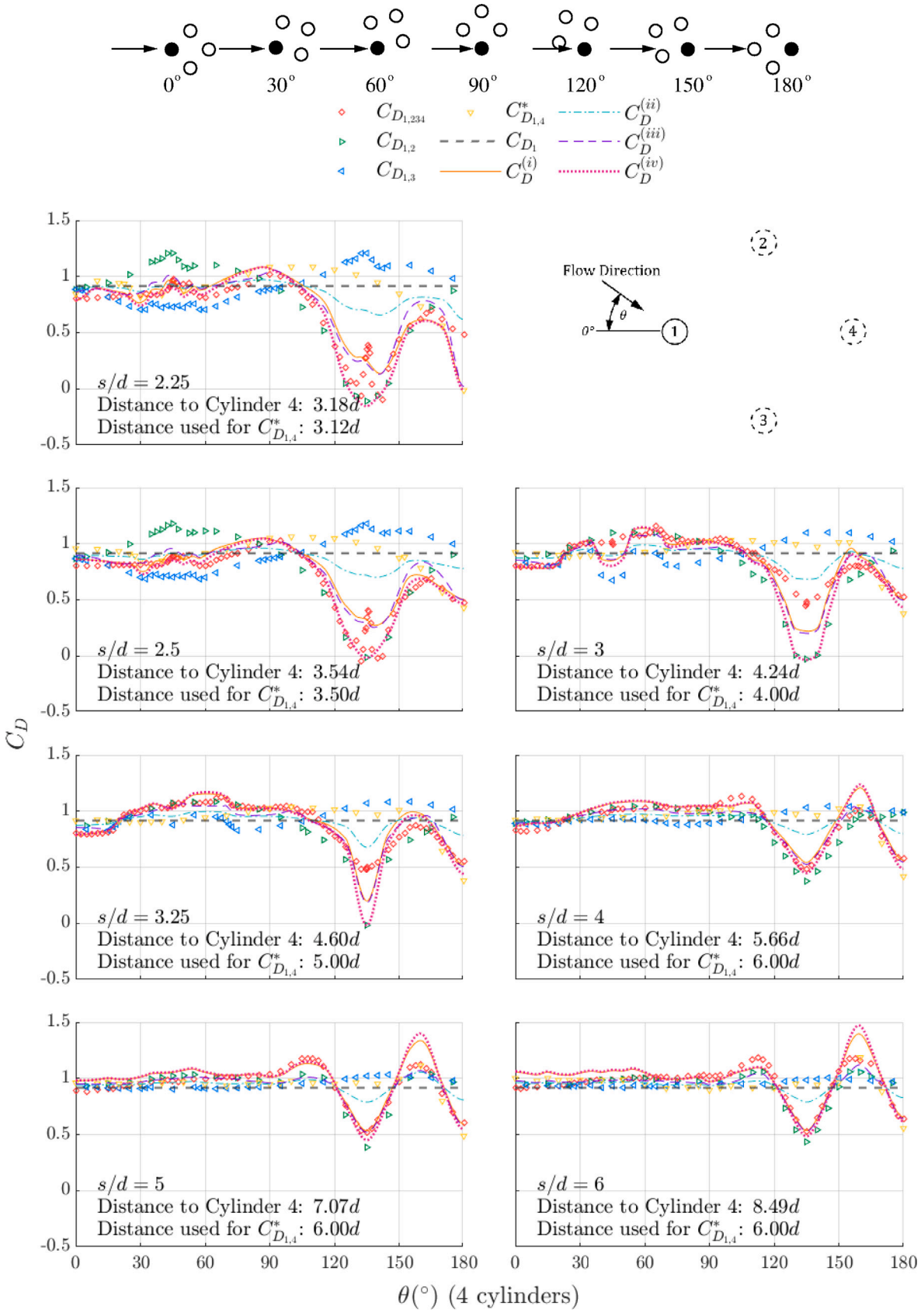

Fig. 25. Comparison of mean drag coefficient variation with θ between individual cylinders within a four-cylinder arrangement and different predictions based on individual cylinders within a two-cylinder arrangement in similar relative positions.

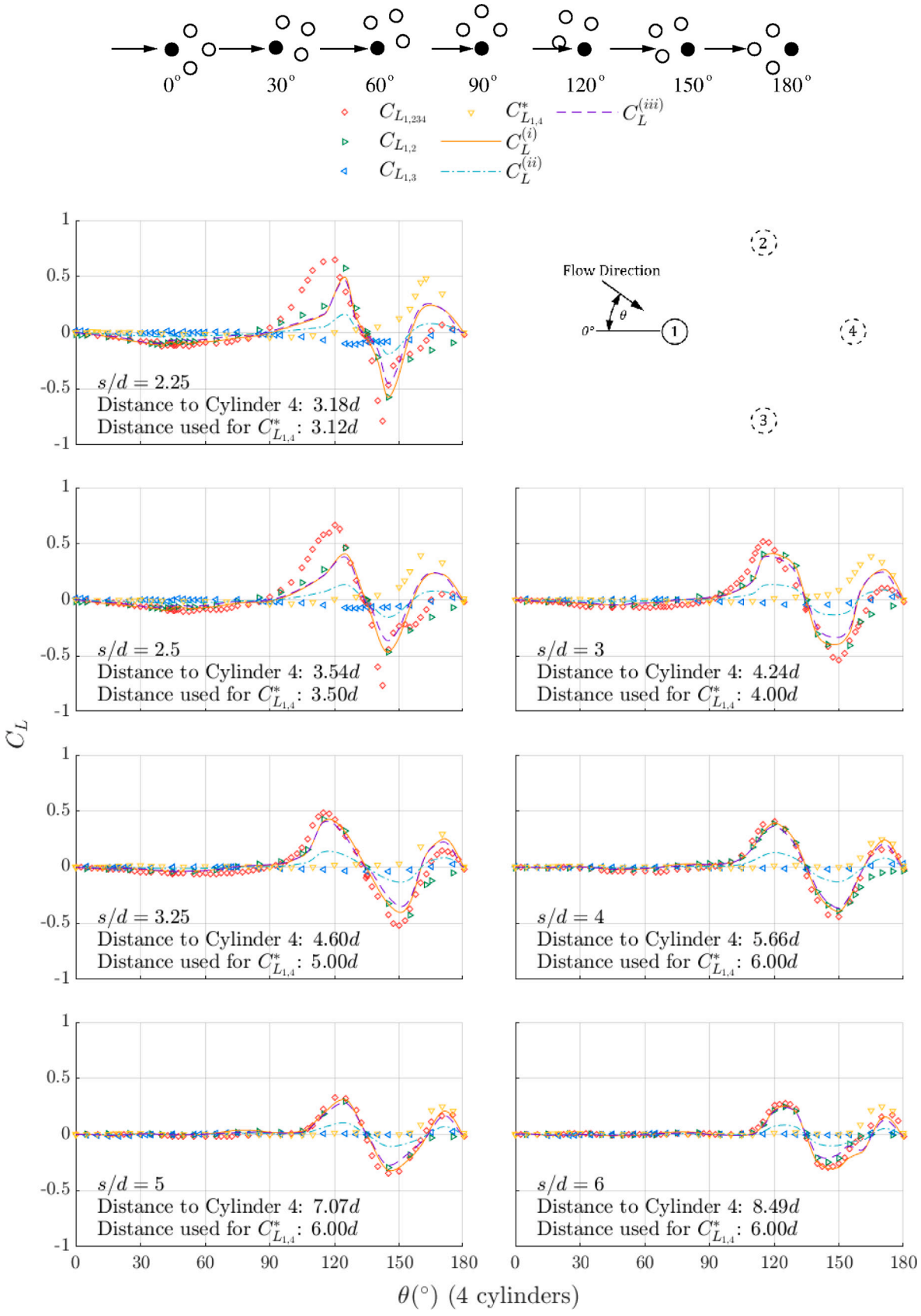

Fig. 26. Comparison of mean lift coefficient variation with θ between individual cylinders within a four-cylinder arrangement and different predictions based on individual cylinders within a two-cylinder arrangement in similar relative positions.

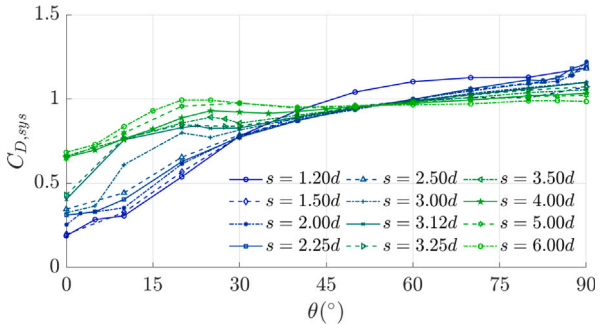

Fig. 27. Variation with θ and s of the combined system drag coefficient of a two-cylinder arrangement.

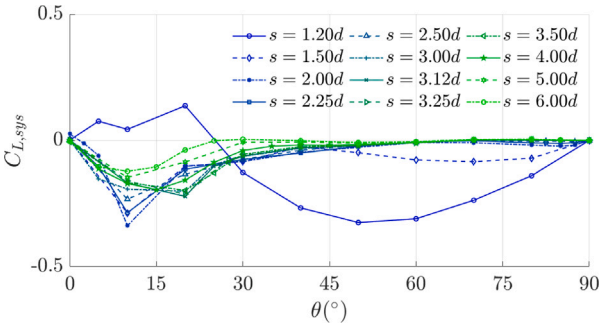

Fig. 28. Variation with θ and s of the combined system lift coefficient of a two-cylinder arrangement.

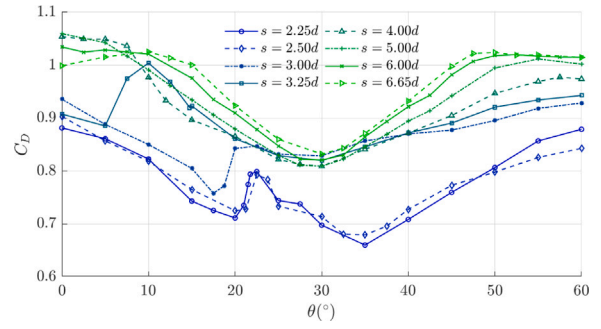

Fig. 29. Variation with θ and s of the combined system drag coefficient of a three-cylinder arrangement.

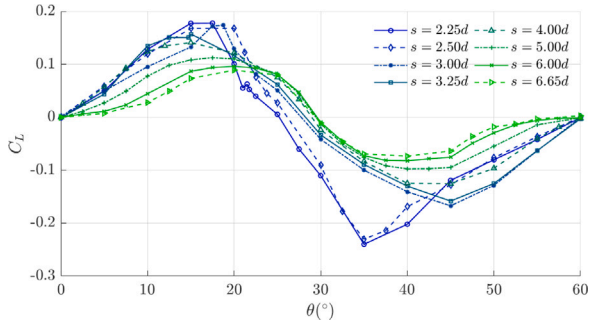

Fig. 30. Variation with θ and s of the combined system lift coefficient of a three-cylinder arrangement.

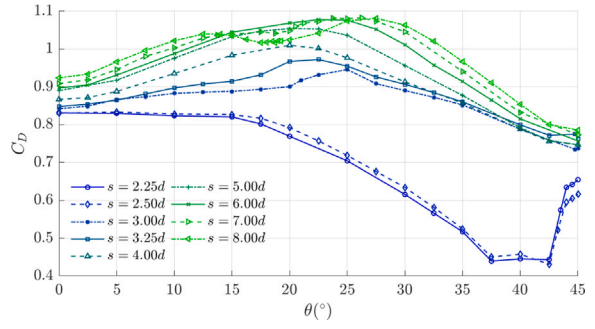

Fig. 31. Variation with θ and s of the combined system drag coefficient of a four-cylinder arrangement.

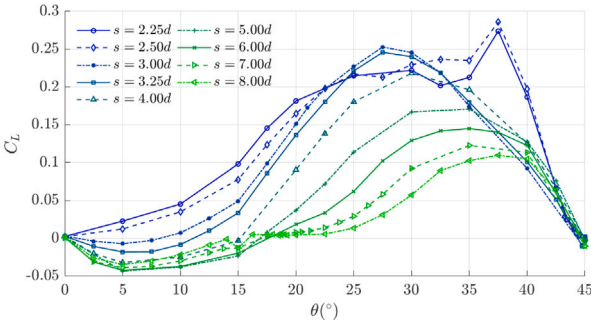

Fig. 32. Variation with θ and s of the combined system lift coefficient of a four-cylinder arrangement.

$s/d = 3$ and 3.25 cases more consistently resembling the higher spacing trends. Notably, this means that whenever cylinder pairs within the system are close to the inline position for these intermediate spacings, the drag trend resembles the larger spacing configurations, which is not the case for the two-cylinder arrangements. The poor estimate of the drag coefficient for these configurations is a consequence of this.

Comparisons between the measured coefficients and estimates of the system force coefficients calculated from the two-cylinder measurements are presented in Figs. 33–36. These are calculated by summing the estimated coefficients for each cylinder within the system (obtained through Eqs. (5) to (8)) and dividing the result by the number of cylinders within the system.

Method (*ii*) generally produces the least accurate predictions, except when two of the cylinders are close to the in-line position for the transitional spacings. As with the individual cylinders, the accuracy of the other methods generally improve as s/d increases. The exception to this is the drag on the four-cylinder arrangement for the two largest spacings, likely due to the previously discussed limitations with extrapolating the data. The implication of this result is that for the highest spacing regime ($s/d \geq 4$), the forces on cylinders within multi-cylinder arrangements can be effectively modelled using data from two-cylinder

arrangements. For smaller spacings, while some configurations can be modelled this way, cross-interference from the additional cylinders limits the range of wind angles over which this can be reliably applied. Configurations where one cylinder is in (or close-to) the wake of another are the most difficult to predict using the methods outlined in this study.

4. Conclusions

This study examined the forces on circular cylinders in two-, three- and four-cylinder arrangements. A comprehensive set of data spanning different wind angles and cylinder spacings is documented for post-critical flow. A comparison is made between these results and earlier sub-critical studies where the broad trends in the force coefficients with spacing and wind angle are shown to persist in post-critical flow, although the magnitudes of the coefficients are different, particularly for the maximum lift coefficient. The results confirm, unsurprisingly, that there are different flow regimes depending on the spacing between the cylinders and the oncoming flow angle. The trends for larger spacings ($s/d \geq 4$) relative to smaller (spacings $2.25 \leq s/d \leq 3$) were distinct. For the intermediate spacings, $3 \leq s/d \leq 3.25$, tended to behave similar to the larger spacings, but for some incidence angles, would bear greater resemblance to the smaller spacings or even display other distinct behaviour.

This research provides a basis for future studies, including numerical simulations on more complex structural arrangements, such as rectangular or diamond shapes. While the focus was on time-averaged loads, understanding time-varying forces is also crucial for certain applications. Limitations of the study include deriving force coefficients from pressure measurements without friction and blockage corrections were not applied. Additionally, all tests were conducted with equally spaced cylinders at a specific turbulence intensity and roughness Reynolds number. Future studies should address these factors in the post-critical regime, particularly at higher turbulence levels, to enhance practical applications for wind-sensitive structures.

Finally, this study compared measured force coefficients with estimates derived from two-cylinder measurements. Method (ii) was the least accurate, except for cases where two cylinders were nearly in-line at transitional spacings. For other methods, accuracy improved as s/d increased, except for the four-cylinder arrangement at the largest spacings due to data extrapolation issues. The results indicate that for large spacings multi-cylinder forces can be modelled using two-cylinder data. For smaller spacings, cross-interference and wake effects reduce the reliability of these models, especially when one cylinder is in the wake of another.

CRediT authorship contribution statement

David Burton: Writing – review & editing, Writing – original draft, Visualization, Validation, Supervision, Software, Resources, Project administration, Methodology, Investigation, Funding acquisition, Formal analysis, Data curation, Conceptualization. **Gershom Easanesan:** Writing – review & editing, Writing – original draft, Visualization, Software, Formal analysis, Data curation. **Anil Pasam:** Writing – review & editing, Methodology, Formal analysis, Data curation. **Christopher Brown:** Visualization, Investigation, Formal analysis, Data curation. **Daniel Tudball Smith:** Writing – review & editing, Validation, Software, Methodology, Formal analysis, Data curation. **Mark C. Thompson:** Writing – review & editing, Supervision, Resources, Project administration, Funding acquisition, Conceptualization.

Declaration of competing interest

The authors declare the following financial interests/personal relationships which may be considered as potential competing interests: Mark Thompson, David Burton reports financial support was provided by Woodside Energy Ltd. Mark Thompson, David Burton reports financial support was provided by Chevron Australia Pty Ltd. If there are other authors, they declare that they have no known competing financial interests or personal relationships that could have appeared to influence the work reported in this paper.

Acknowledgements

This research was supported by the Australian Government through the Australian Research Council's Linkage Projects funding scheme, LP180100234.

Appendix. Revisiting previous results using newly introduced superposition approaches

In addition to the data presented in this study, the force coefficient prediction approaches discussed were also applied to the three-cylinder results presented by Price and Paidoussis (1984). The results from this exercise for the lift and drag are presented in Figs. 37 and 38, respectively, noting that C_D^i, C_D^{ii} and C_L^i had previously been computed by Price and Paidoussis themselves.

In general, the trends in both lift and drag are reasonably well predicted by all methods except method (ii) when the side-by-side cylinders are $4d$ away from each other. For the cases considered here, the most accurate predictions were obtained when $l/d = 5$. $C_D^{(i)}$ and $C_D^{(iv)}$ both underestimate the drag when $l/d = 1.5$, although method (iii) performs well here. None of the methods predict the maximum lift coefficient for $l/d = 1.5$, while when $l/d = -1.5$, method (ii) outperforms the other methods for small values of y/d in predicting the lift coefficient.

When the gap between the side-by-side cylinders is reduced to $1.5d$, the predictions are significantly worse. For $l/d = 5$, the drag at larger values of y/d are predicted well by methods (i), (ii) and (iv), with method (i) also accurately predicting the minimum drag. For the $l/d = 1.5$ case, $C_D^{(iv)}$ produces reasonable estimates when y/d is small, but all the methods are generally poor predictors outside this. Reasonable predictions of the lift coefficients were obtained for these cases for large values of y/d (i.e., when the metric cylinder moves outside the line of the side-by-side cylinders). However, as y/d gets smaller, all methods fail to predict the trends in lift. $C_D^{(i)}$ and $C_D^{(iii)}$ recover the trend well when y/d is close to zero for the $l/d = 1.5$ case, but not for the other spacings.

The results here suggest that the methods used in this study to predict the forces on larger numbers of cylinders based on one- and two-cylinder data remain viable for sub-critical flow and non-equidistant arrangements. However, like the equidistant cases, they do not produce accurate predictions for closely-spaced cylinders for configurations where cylinder-wake interactions are prominent.

Data availability

Data will be made available on request.

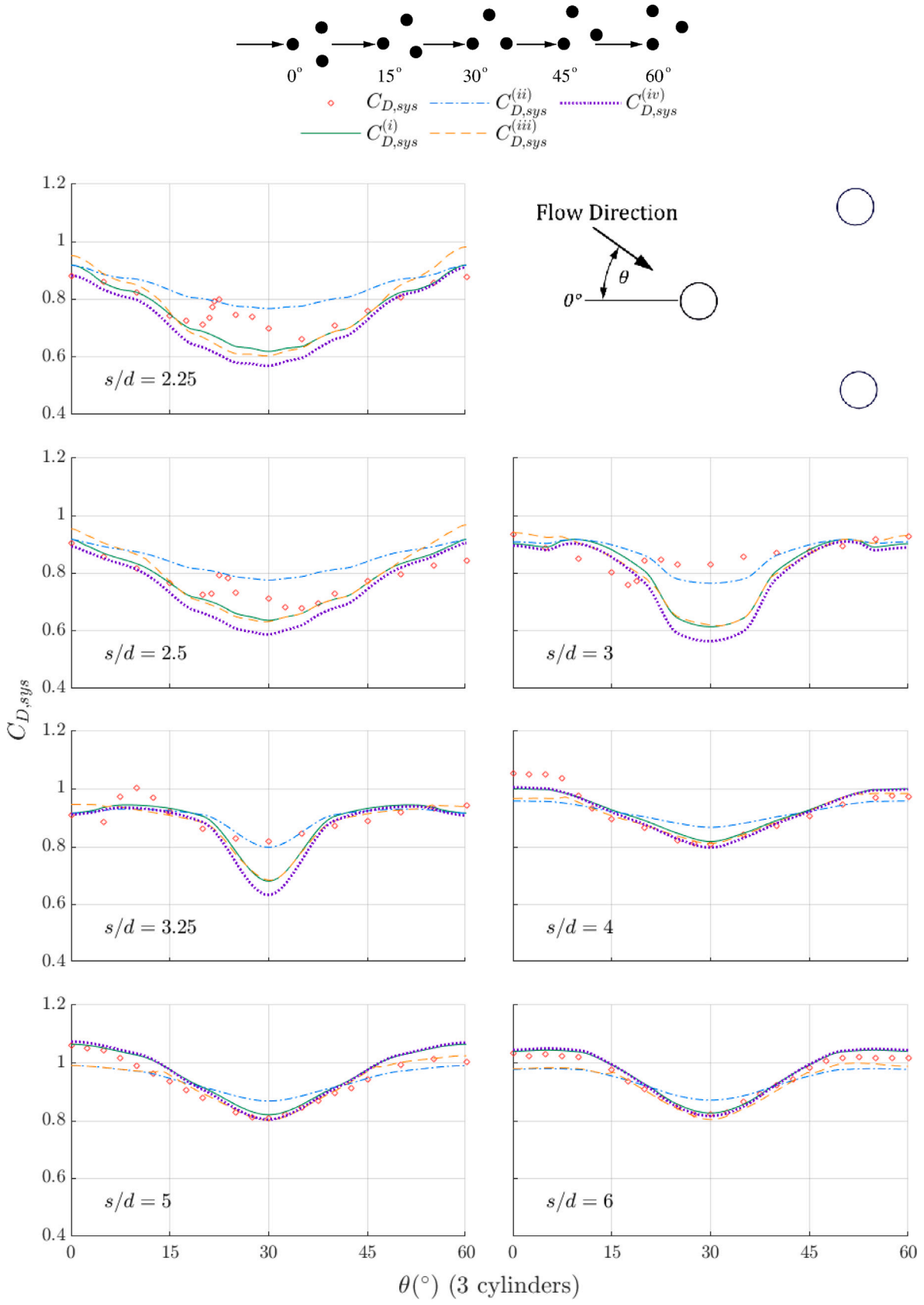

Fig. 33. Comparison of mean drag coefficient variation with θ between a system of cylinders within a three-cylinder arrangement different predictions based on individual cylinders within a two-cylinder arrangement in similar relative positions.

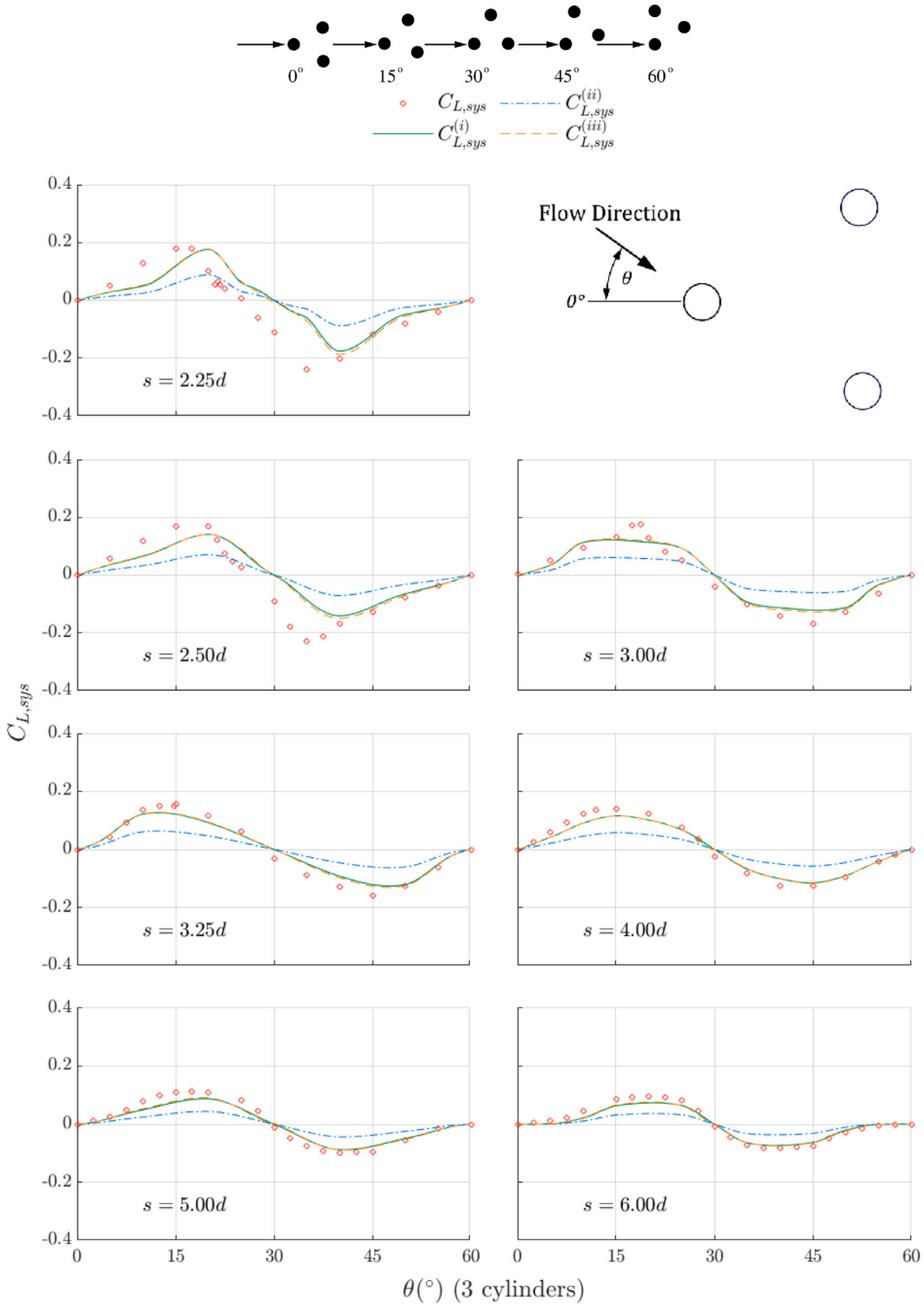

Fig. 34. Comparison of mean lift coefficient variation with θ between individual cylinders within a three-cylinder arrangement and different predictions based on individual cylinders within a two-cylinder arrangement in similar relative positions.

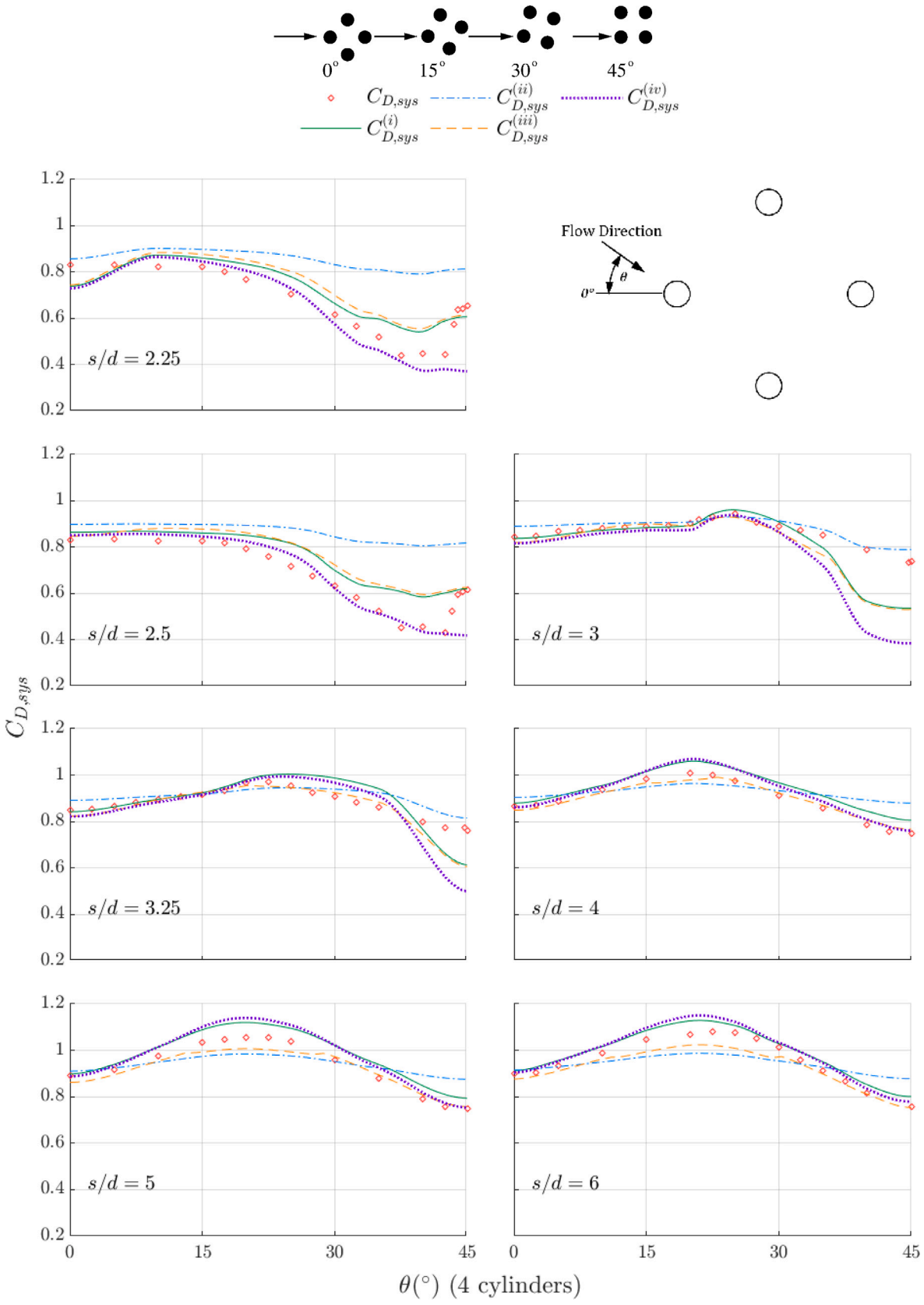

Fig. 35. Comparison of mean drag coefficient variation with θ between a system of cylinders within a four-cylinder arrangement different predictions based on individual cylinders within a two-cylinder arrangement in similar relative positions.

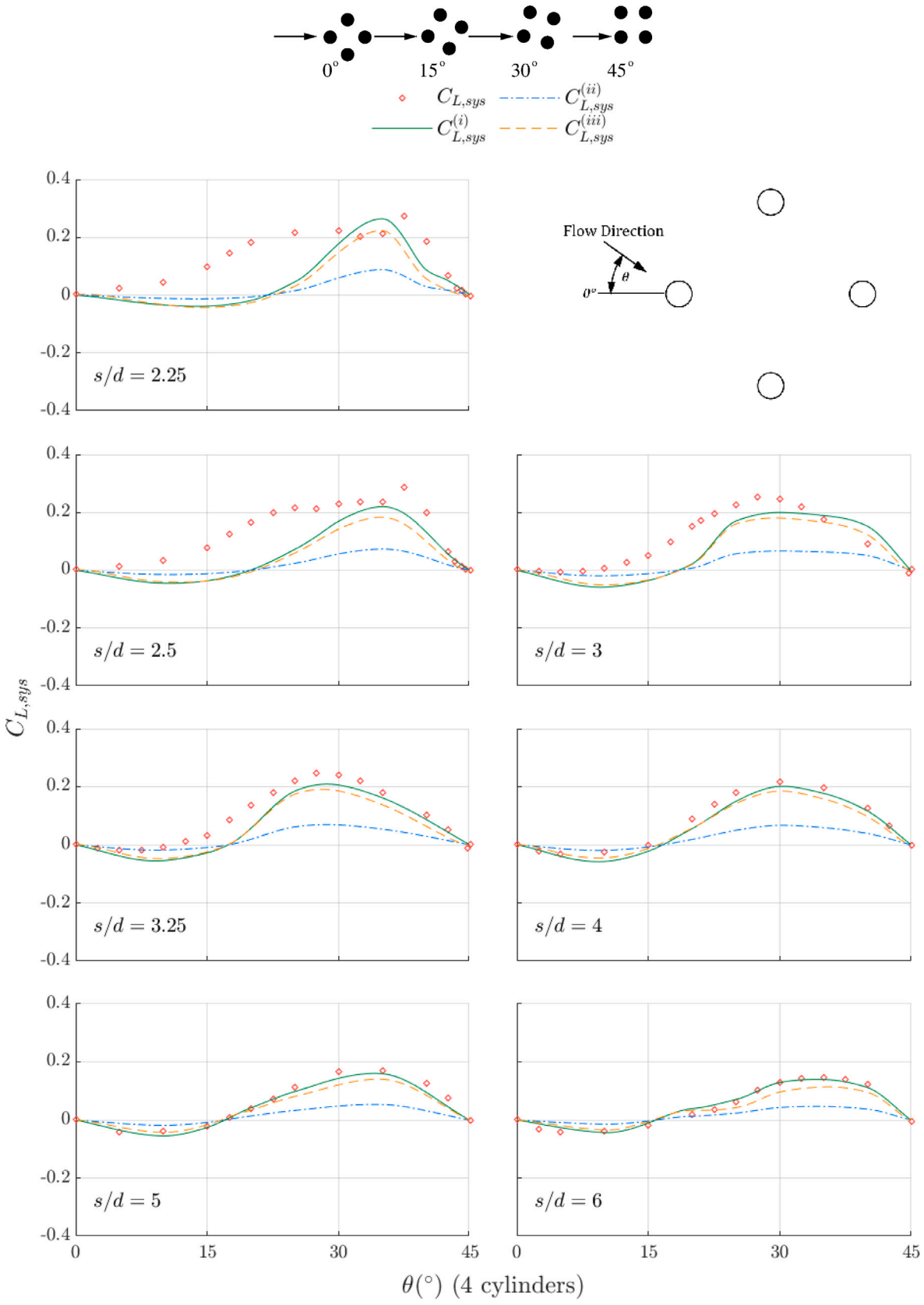

Fig. 36. Comparison of mean lift coefficient variation with θ between individual cylinders within a four-cylinder arrangement and different predictions based on individual cylinders within a two-cylinder arrangement in similar relative positions.

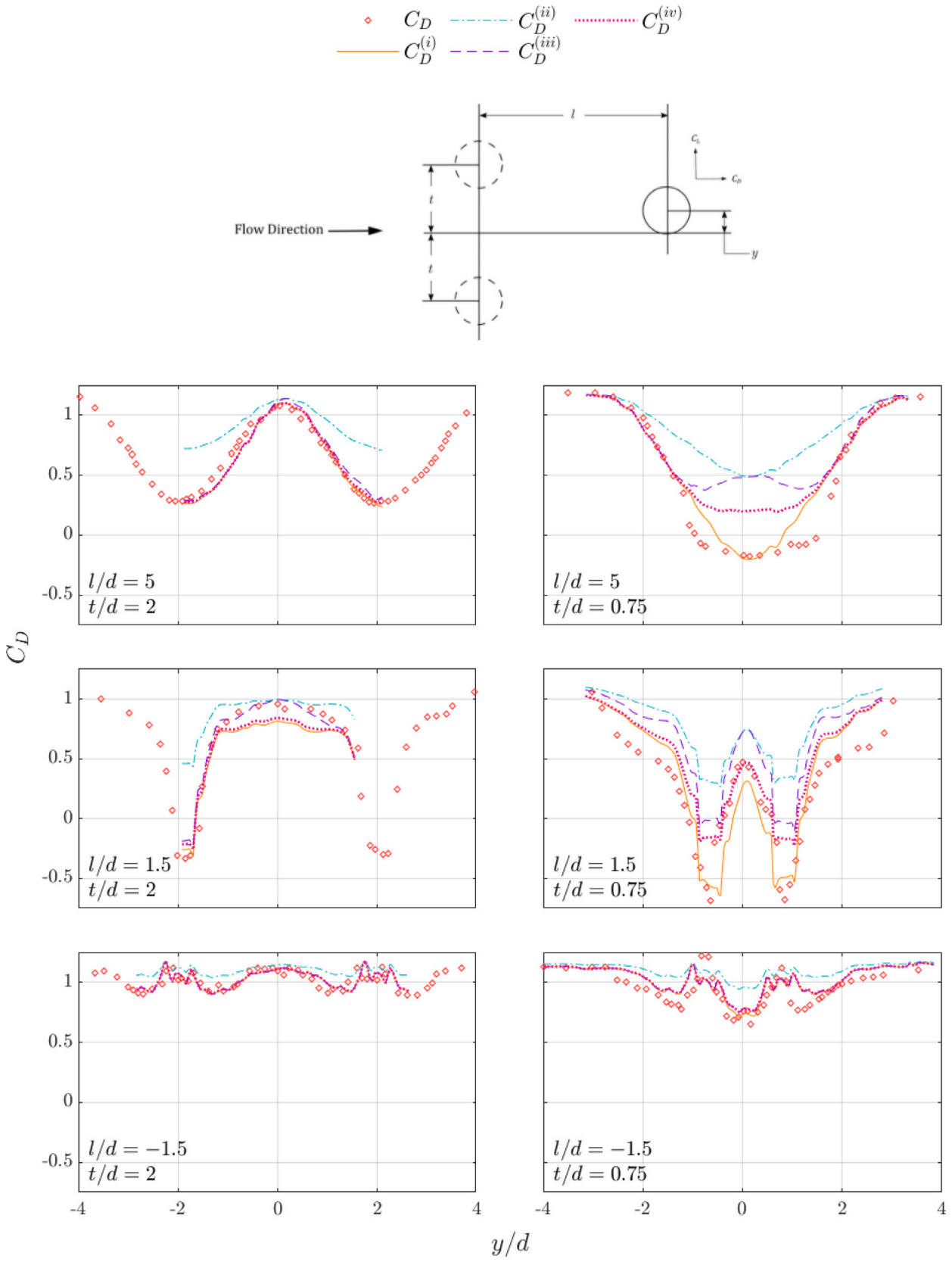

Fig. 37. Re-evaluation of drag coefficients on a cylinder in the vicinity of two side-by-side cylinders from Price and Paidoussis (1984) using different superposition methods. Negative values for l/d indicate that the cylinder is upstream of the side-by-side cylinders.

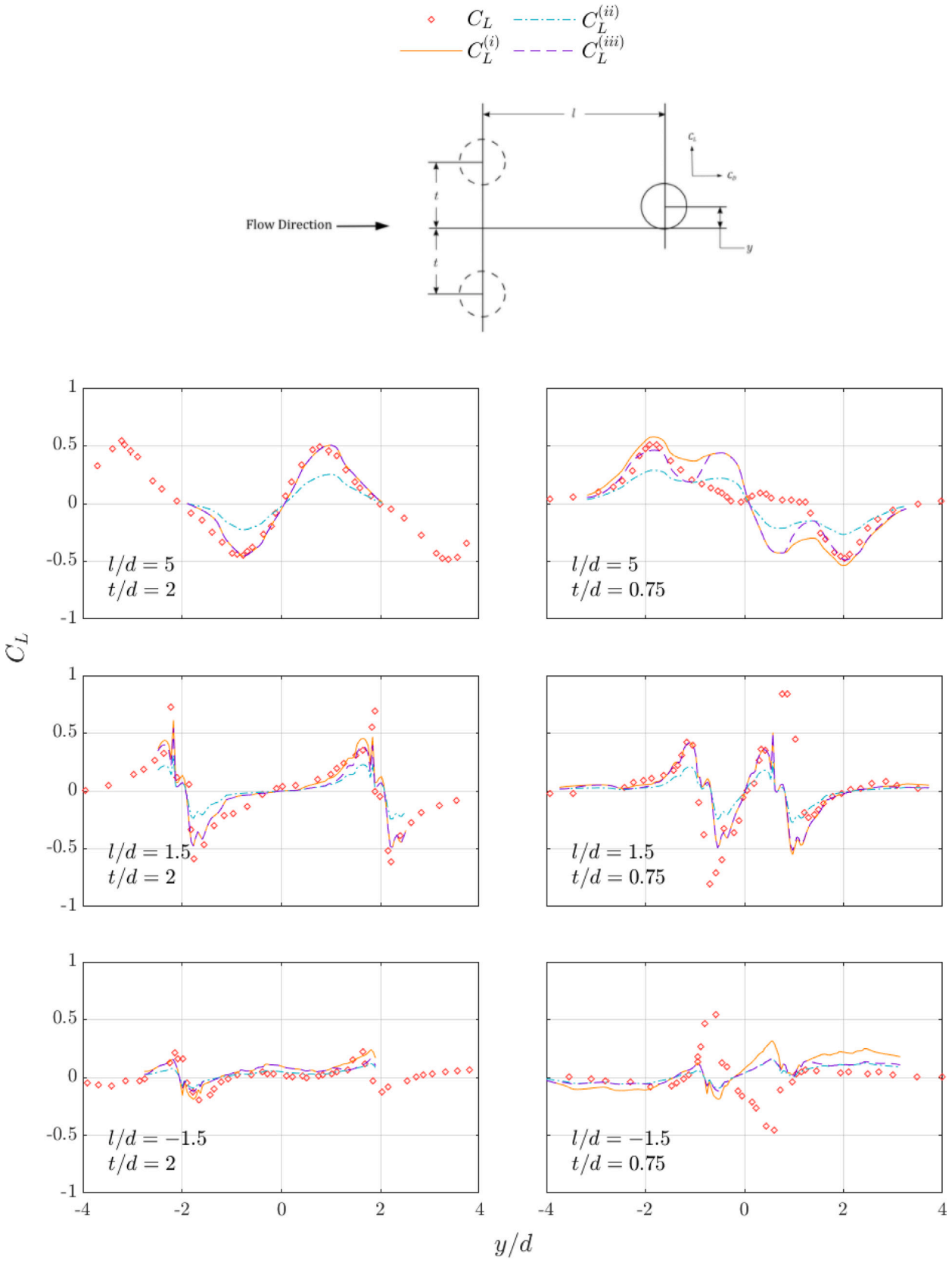

Fig. 38. Re-evaluation of lift coefficients on a cylinder in the vicinity of two side-by-side cylinders from Price and Paidoussis (1984) using different superposition methods. Negative values for l/d indicate that the cylinder is upstream of the side-by-side cylinders.

References

Achenbach, E., 1971. Influence of surface roughness on the cross-flow around a circular cylinder. J. Fluid Mech. 46 (2), 321–335. http://dx.doi.org/10.1017/S0022112071000569.

Achenbach, E., Heinecke, E., 1981. On vortex shedding from smooth and rough cylinders in the range of Reynolds numbers 6×10^3 to 5×10^6. J. Fluid Mech. 109, 239–251. http://dx.doi.org/10.1017/S002211208100102X.

Alam, M.M., Moriya, M., Sakamoto, H., 2003a. Aerodynamic characteristics of two side-by-side circular cylinders and application of wavelet analysis on the switching phenomenon. J. Fluids Struct. 18 (3–4), 325–346. http://dx.doi.org/10.1016/j.jfluidstructs.2003.07.005.

Alam, M.M., Moriya, M., Takai, K., Sakamoto, H., 2003b. Fluctuating fluid forces acting on two circular cylinders in a tandem arrangement at a subcritical Reynolds number. J. Wind Eng. Ind. Aerodyn. 91 (1–2), 139–154. http://dx.doi.org/10.1016/S0167-6105(02)00341-0.

Bergh, H., Tijdeman, H., 1965. Theoretical and Experimental Results for the Dynamic Response of Pressure Measuring Systems. Tech. Rep. NLR-TR F.238, Nationaal Lucht- en Ruimtevaartlaboratorium.

Dubois, R., Andrianne, T., 2022. Flow around tandem rough cylinders: Effects of spacing and flow regimes. J. Fluids Struct. 109, 103465. http://dx.doi.org/10.1016/j.jfluidstructs.2021.103465, URL: https://www.sciencedirect.com/science/article/pii/S0889974621002292.

Fage, A., Warsap, J., 1929. The Effects of Turbulence and Surface Roughness on the Drag of a Circular Cylinder. Reports and Memoranda No. 1283, Aeronautical Research Committee.

Gu, Z., 1996. On interference between two circular cylinders at supercritical Reynolds number. J. Wind Eng. Ind. Aerodyn. 62 (2–3), 175–190. http://dx.doi.org/10.1016/s0167-6105(96)00056-6.

Gu, Z., Sun, T., 1999. On interference between two circular cylinders in staggered arrangement at high subcritical Reynolds numbers. J. Wind Eng. Ind. Aerodyn. 80 (3), 287–309. http://dx.doi.org/10.1016/s0167-6105(98)00205-0.

Gu, Z., Sun, T., 2001. Classifications of flow pattern on three circular cylinders in equilateral-triangular arrangements. J. Wind Eng. Ind. Aerodyn. 89 (6), 553–568. http://dx.doi.org/10.1016/s0167-6105(00)00091-x.

Ljungkrona, L., Norberg, C., Sundén, B., 1991. Free-stream turbulence and tube spacing effects on surface pressure fluctuations for two tubes in an in-line arrangement. J. Fluids Struct. 5 (6), 701–727. http://dx.doi.org/10.1016/0889-9746(91)90364-u.

Niemann, H.J., Hölscher, N., 1990. A review of recent experiments on the flow past circular cylinders. J. Wind Eng. Ind. Aerodyn. 33 (1–2), 197–209. http://dx.doi.org/10.1016/0167-6105(90)90035-b.

Pasam, A., Smith, D.T., Burton, D., Thompson, M.C., 2024. Flow over two inline rough cylinders in the postcritical regime. Phys. Fluids 36 (9), 095145. http://dx.doi.org/10.1063/5.0221390.

Pasam, A., Smith, D.T., Holmes, J.D., Burton, D., Thompson, M.C., 2023. The influence of surface roughness on postcritical flow over circular cylinders revisited. J. Fluid Mech. 975, E1. http://dx.doi.org/10.1017/jfm.2023.846.

Price, S.J., Paidoussis, M.P., 1984. The aerodynamic forces acting on groups of two and three circular cylinders when subject to a cross-flow. J. Wind Eng. Ind. Aerodyn. 17 (3), 329–347. http://dx.doi.org/10.1016/0167-6105(84)90024-2.

Roshko, A., 1961. Experiments on the flow past a circular cylinder at very high Reynolds number. J. Fluid Mech. 10 (3), 345–356. http://dx.doi.org/10.1017/S0022112061000950.

Sayers, A.T., 1987. Flow interference between three equispaced cylinders when subjected to a cross flow. J. Wind Eng. Ind. Aerodyn. 26, 1–19.

Sayers, A.T., 1988. Flow interference between four equispaced cylinders when subjected to a cross flow. J. Wind Eng. Ind. Aerodyn. 31 (31), 9–28.

Spiedel, L., 1954. Einfluss der oberflächenrauhigkeit auf die strömungsverluste in ebenen schaufelgittern. Forsch. Gebiet Ingen. 20, 129–140.

Sumner, D., 2010. Two circular cylinders in cross-flow: A review. J. Fluids Struct. 26 (6), 849–899. http://dx.doi.org/10.1016/j.jfluidstructs.2010.07.001.

Sumner, D., Richards, M.D., Akosile, O.O., 2005. Two staggered circular cylinders of equal diameter in cross-flow. J. Fluids Struct. 20 (2), 255–276. http://dx.doi.org/10.1016/j.jfluidstructs.2004.10.006.

Szechenyi, E., 2006. Supercritical Reynolds number simulation for two-dimensional flow over circular cylinders. J. Fluid Mech. 70 (3), 529–542. http://dx.doi.org/10.1017/s0022112075002170.

Tatsuno, M., Amamoto, H., Ishi-i, K., 1998. Effects of interference among three equidistantly arranged cylinders in a uniform flow. Fluid Dyn. Res. 22 (5), 297–315. http://dx.doi.org/10.1016/s0169-5983(97)00040-3.

Wang, P., Zhou, Q., Alam, M.M., Yang, Y., Li, M., 2022. Effects of streamwise gust amplitude on the flow around and forces on two tandem circular cylinders. Ocean Eng. 261, 112040. http://dx.doi.org/10.1016/j.oceaneng.2022.112040, URL: https://www.sciencedirect.com/science/article/pii/S0029801822013701.

Zdravkovich, M.M., 1977. Review of flow interference between two circular cylinders in various arrangements. J. Fluids Eng. 99 (4), 618–633. http://dx.doi.org/10.1115/1.3448871.

Zhou, Y., Alam, M.M., 2016. Wake of two interacting circular cylinders: A review. Int. J. Heat Fluid Flow 62, 510–537. http://dx.doi.org/10.1016/j.ijheatfluidflow.2016.08.008.

Zhou, Y., Hao, J., Alam, M.M., 2024. Wake of two tandem square cylinders. J. Fluid Mech. 983, A3. http://dx.doi.org/10.1017/jfm.2024.119.